Impurity in a granular gas under nonlinear Couette flow

Francisco Vega Reyes, Vicente Garzó and Andrés Santos

Departamento de Física, Universidad de Extremadura, E-06071 Badajoz, Spain
E-mail: fvega@unex.es, vicenteg@unex.es and andres@unex.es
URL: http://www.unex.es/eweb/fisteor/vicente/ and
http://www.unex.es/eweb/fisteor/andres/

Abstract. We study in this work the transport properties of an impurity immersed in a granular gas under stationary nonlinear Couette flow. The starting point is a kinetic model for low-density granular mixtures recently proposed by the authors (Vega Reyes *et al* 2007 *Phys. Rev.* E **75** 061306). Two routes have been considered. First, a hydrodynamic or normal solution is found by exploiting a formal mapping between the kinetic equations for the gas particles and for the impurity. We show that the transport properties of the impurity are characterized by the ratio between the temperatures of the impurity and gas particles and by five generalized transport coefficients: three related to the momentum flux (a nonlinear shear viscosity and two normal stress differences) and two related to the heat flux (a nonlinear thermal conductivity and a cross-coefficient measuring a component of the heat flux orthogonal to the thermal gradient). Second, by means of a Monte Carlo simulation method we numerically solve the kinetic equations and show that our hydrodynamic solution is valid in the bulk of the fluid when realistic boundary conditions are used. Furthermore, the hydrodynamic solution applies to arbitrarily (inside the continuum regime) large values of the shear rate, of the inelasticity, and of the rest of the parameters of the system. Preliminary simulation results of the true Boltzmann description show the reliability of the nonlinear hydrodynamic solution of the kinetic model. This shows again the validity of a hydrodynamic description for granular flows, even under extreme conditions, beyond the Navier–Stokes domain.

1742-5468/08/P09003+30$30.00

J. Stat. Mech. (2008) P09003

Contents

1. Introduction

The understanding of transport processes occurring in granular mixtures is still challenging. In the low- and moderate-density regimes the Boltzmann and Enskog equations, suitably adapted to account for inelastic collisions, have proven to provide an adequate framework for the study of granular flows [1, 2]. In particular, if the spatial gradients present in the system are weak, the Navier–Stokes (NS) constitutive equations for the fluxes of mass, momentum and energy have been derived (with explicit expressions for the transport coefficients) for the model of inelastic hard spheres characterized by constant coefficients of normal restitution α_{ij}. Most of the early derivations were restricted to the quasi-elastic limit ($\alpha_{ij} \approx 1$), thus assuming an expansion around Maxwellians at the *same* temperature [3]–[8]. However, the nonequipartition of energy becomes significant beyond the quasi-elastic limit, as confirmed by kinetic theory [9]–[12], computer simulations [11], [13]–[21] and real experiments [21]–[23]. A more realistic derivation of the NS transport coefficients [24]–[27] requires taking into account the nonequipartition of energy and applies for finite dissipation. The accuracy of this latter approach has
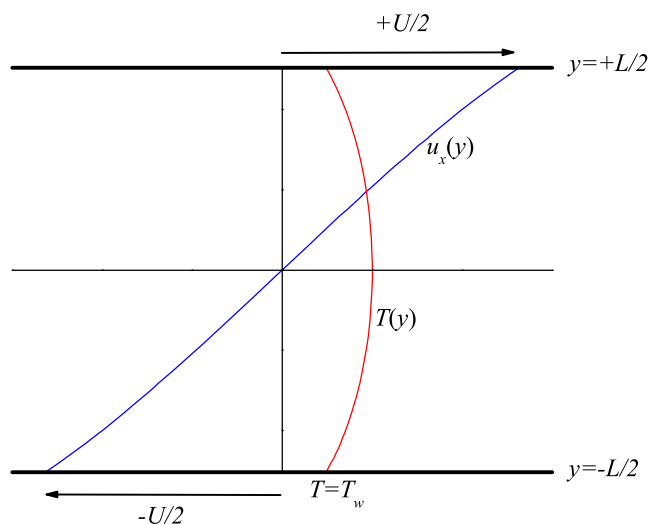
Figure 1. Sketch of a planar Couette flow. The gas is enclosed between two infinite parallel walls located at $y = \pm L/2$, moving along the x direction with velocities $\pm U/2$, and kept at the temperature T_{w}.

been confirmed by computer simulations in the cases of the diffusion [28, 29] and shear viscosity [30, 31] coefficients. On the other hand, the practical applicability of the NS equations is limited to small spatial gradients, while many steady granular flows do not fulfill in general this condition, due to the coupling between inelasticity and gradients [1, 32].

The physical situation we study in this work corresponds to a gas of inelastic hard spheres enclosed between two parallel walls at $y = \pm L/2$ moving with velocities $\pm U/2$ along the x axis and kept, in general, at different temperatures $T_{\pm}$ [33]–[38]. In the base steady state the flow velocity is along the x axis and the hydrodynamic fields depend on the y variable only (planar Couette flow). This macroscopic state is characterized by a combined momentum and heat transport described by the pressure tensor $P_{ij}(y)$ and the heat flux $\mathbf{q}(y)$, respectively. A sketch of the geometry of the steady planar Couette flow for the symmetric choice $T_{+} = T_{-} = T_{\mathrm{w}}$ is given in figure 1.

Since granular matter is generally present in polydisperse form, the study of the Couette flow in the case of a granular mixture is an interesting problem from a fundamental and practical point of view. Needless to say, the general problem is quite intricate since not only the number of parameters (masses, sizes, composition and coefficients of restitution) but also the number of transport coefficients are higher than in the monocomponent case. As a first step, and to gain some insight into the general problem, in this paper we consider the tracer limit case, namely a binary mixture where the mole fraction of one of the components (tracer species, denoted by label 1) is much smaller than that of the other component (excess species, denoted by label 2). In this tracer limit, the state of the excess species is unaffected by the presence of the tracer particles and so its velocity distribution function f_2 obeys a closed Boltzmann equation in the low-density regime. In addition, the mutual collisions among the tracer particles can be neglected versus the tracer-gas collisions, so that the tracer velocity distribution function f_1 obeys a linear (inelastic) Boltzmann–Lorentz equation. This problem is formally equivalent to that of

an impurity or intruder immersed in a granular gas, and this will be the terminology used in this paper. Since the impurity particle is assumed to be mechanically different from the gas particles, the dimensionless parameters characterizing the mixture are the coefficients of restitution α_{12} and α_{22}, the mass ratio m_1/m_2 and the size ratio σ_1/σ_2.

Unfortunately, the complexity of the nonlinear Couette flow makes its treatment at the level of the Boltzmann equation practically unattainable, even in the monocomponent case. Thus, here we will consider a model kinetic equation recently proposed for granular mixtures [39]. In the tracer limit, this kinetic model reduces to the same closed kinetic equation for the excess species as considered in [37] plus a Boltzmann–Lorentz-like kinetic equation for the impurity particle. The kinetic equation for f_2 admits an *exact* solution for the steady planar Couette flow [37]. Exploiting the formal analogy between the kinetic equations for f_1 and f_2, we find in this paper an exact solution for f_1. This solution allows us to obtain the most relevant velocity moments of f_1, which are directly related to the momentum and heat fluxes associated with the impurity. In particular, as expected, the impurity temperature clearly differs from the granular temperature of the gas particles, showing again the breakdown of the energy equipartition in nonequilibrium states.

The exact solution found here qualifies as a 'normal' or hydrodynamic solution since f_1 and f_2 depend on space only through an explicit functional dependence on the hydrodynamic fields. This hydrodynamic description applies even at strong dissipation (i.e. beyond the quasi-elastic limit) and strong inhomogeneity (i.e. beyond the NS domain), as long as the densest regions of the system remain sufficiently dilute and the molecular chaos assumption holds. This provides a counterexample against the speculation that a hydrodynamic description for granular flows is limited to weak dissipation and/or weak inhomogeneities. In order to assess the reliability of this hydrodynamic solution, we have also solved the model kinetic equation by means of Monte Carlo simulations with Couette-flow boundary conditions. Comparison with the hydrodynamic solution shows that the latter is not a mathematical artifact but applies in the bulk region of the system, where boundary effects are negligible. This agreement between theory and simulations holds for system sizes L as small as a few mean free paths.

In order to gain some insight into the expected hydrodynamic fields in the Couette problem, let us consider first a monocomponent granular gas. In this case, the exact energy and momentum balance equations yield

$$\frac{2}{dn}\left(P_{xy}\frac{\partial u_x}{\partial y} + \frac{\partial q_y}{\partial y} \right) = -\zeta T, \tag{1.1}$$

$$\frac{\partial P_{xy}}{\partial y} = 0, \tag{1.2}$$

$$\frac{\partial P_{yy}}{\partial y} = 0, \tag{1.3}$$

where $d = 2$ and 3 for hard discs and spheres, respectively, n is the number density and ζ is the cooling rate due to the inelastic character of collisions. By dimensional analysis in the dilute limit, $\zeta = \nu \zeta^*(\alpha)$, where $\nu \propto nT^{1/2}$ is an effective collision frequency for hard spheres. Equations (1.1)–(1.3) do not constitute a closed set of equations for the hydrodynamic fields $n(y)$, $T(y)$ and $u_x(y)$, unless the constitutive equations expressing the fluxes as functionals of the hydrodynamic fields are known. For illustration, let us

assume for the moment that the hydrodynamic gradients are small enough so as to justify the use of the NS constitutive equations. Due to the geometry of the problem, at NS order we have $P_{xx} = P_{yy} = P_{zz} = p$ [40, 41], from which, with (1.3), it immediately follows that the hydrostatic pressure $p = nT$ is constant, i.e.

$$p = \text{const.} \tag{1.4}$$

Moreover, the NS constitutive equations imply that $q_x = q_z = 0$ and

$$P_{xy} = -\eta \frac{\partial u_x}{\partial y}, \qquad q_y = -\kappa \frac{\partial T}{\partial y} - \mu \frac{\partial n}{\partial y}, \tag{1.5}$$

where $\eta = (p/\nu)\eta^*(\alpha)$ is the shear viscosity, $\kappa = (p/m\nu)\kappa^*(\alpha)$ is the thermal conductivity (m being the mass of a particle) and $\mu = (T^2/m\nu)\mu^*(\alpha)$ is a transport coefficient absent in the elastic case ($\alpha = 1$). The explicit form of the dimensionless functions $\zeta^*(\alpha)$, $\eta^*(\alpha)$, $\kappa^*(\alpha)$ and $\mu^*(\alpha)$ is known [40, 41]. Insertion of equations (1.4) and (1.5) into equations (1.1) and (1.2) yields

$$a \equiv \frac{1}{\nu}\frac{\partial u_x}{\partial y} = \text{const}, \tag{1.6}$$

$$\frac{1}{2m}\left(\frac{1}{\nu}\frac{\partial}{\partial y}\right)^2 T = -\gamma = \text{const.} \tag{1.7}$$

Therefore, according to the NS description, the local shear rate $\partial u_x/\partial y$ scaled with the local collision frequency $\nu \propto p/T^{1/2}$ is a constant, and the temperature profile is such that $(\nu^{-1}\partial_y)^2 T$ is a constant that depends on the reduced shear rate a and the coefficient of restitution α. The set of NS base steady states in the system have been analytically solved in a recent work [42].

As said before, due to inelasticity these steady states do not have small spatial gradients (except for $\alpha \approx 1$ [42]) and thus a kinetic description beyond the NS domain is in general required in order to properly describe granular Couette flows. Specifically, this is even more necessary if $\gamma \geq 0$ (and this happens when the viscous heating dominates over collisional cooling [32]), since in this case the Knudsen number is always greater than the one for $\gamma < 0$ [42]. Such a description of the Couette flow beyond the NS domain was carried out in [37] for a monocomponent granular gas with $\gamma \geq 0$. Interestingly enough, this solution shares with the NS description the structure of the hydrodynamic profiles (1.4), (1.6) and (1.7). However, in the constitutive equations, the transport coefficients and the parameter γ are *nonlinear* functions of the shear rate a [37]. At the same time, the solution is also able to capture normal stress differences ($P_{xx} \neq P_{yy} \neq P_{zz}$) and the component of the heat flux along the flow direction ($q_x \neq 0$), which are all nonlinear effects [37]. All theoretical results in [37] compare well with Monte Carlo simulations of the Boltzmann equation, showing the reliability of the kinetic model beyond the quasi-elastic limit. As an illustrative example of the necessity of a nonlinear description, we briefly analyze the case $\gamma = 0$, which occurs for a threshold value of a that, in the NS description, is $a_{\text{th}}^{\text{NS}}(\alpha) = \sqrt{d\zeta^*(\alpha)/2\eta^*(\alpha)}$ and in the nonlinear Couette flow is $a_{\text{th}}(\alpha) = \sqrt{d\zeta^*(\alpha)/2}[1 + \zeta^*(\alpha)]$ [37]. We show in figure 2 the disagreement between both values, which becomes very apparent for values far from the quasi-elastic limit. As shown in [37], the nonlinear prediction $a_{\text{th}}(\alpha)$ agrees very well with Monte Carlo simulations of the Boltzmann equation.
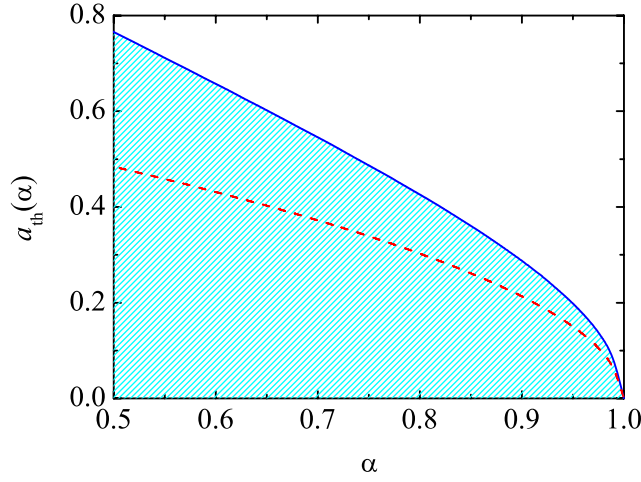
Figure 2. Plot of the threshold value of the reduced shear rate, $a_{\mathrm{th}}(\alpha)$, for a three-dimensional granular gas in the planar Couette flow. The dashed line is the result $a_{\mathrm{th}}^{\mathrm{NS}}(\alpha) = \sqrt{d\zeta^*(\alpha)/2\eta^*(\alpha)}$ obtained from the NS equations, while the solid line is the prediction $a_{\mathrm{th}}(\alpha) = \sqrt{d\zeta^*(\alpha)/2}[1 + \zeta^*(\alpha)]$ from an exact solution of a kinetic model of the Boltzmann equation [37]. The separation between both curves is a measure of the limitations of the NS description.

We propose in this work a theoretical solution of the nonlinear hydrodynamic profiles for the impurity that exhibits absence of mutual diffusion (i.e. flow velocities are equal for impurity and excess components). Furthermore, this solution for the impurity also obeys equations of the form (1.4), (1.6) and (1.7). We will use a numerical solution of the kinetic equation by a Monte Carlo method in order to show that the theoretical solution we propose matches the hydrodynamic profiles and transport coefficients that result from the kinetic equation. Furthermore, with the use of the numerical solution we show that the hypotheses, notably the absence of mutual diffusion, used in order to find our hydrodynamic solution are actually always true in a wide range of system parameters (including shear rate and inelasticity). In addition, we present preliminary Monte Carlo simulations of the Boltzmann equations which confirm the hydrodynamic profiles predicted by the nonlinear hydrodynamic solution of the kinetic model.

This paper is organized as follows. The kinetic model for the mixture is described in section 2. Then, the physical problem we are interested in is introduced. Section 3 presents the exact hydrodynamic solution to the kinetic equations for f_1 and f_2, with explicit expressions for the heat and momentum fluxes of both species. The simulation method is described in section 4 and comparisons between the theoretical predictions and the simulation results are carried out in section 5. Finally, the results are summarized and discussed in section 6.

2. Kinetic model for granular mixtures

Let us consider a mixture composed by smooth inelastic discs ($d = 2$) or spheres ($d = 3$) of masses m_i and diameters σ_i, the inelasticity of collisions between a sphere of species i and a sphere of species j being characterized by a constant coefficient of restitution

$0 < \alpha_{ij} \le 1$. We will focus on the dilute limit, i.e. the mean free path of the particles is much larger than their sizes. The relevant hydrodynamic fields are the number densities n_i, the flow velocity $\mathbf{u}$ and the temperature T. They are defined in terms of moments of the velocity distribution functions $f_i(\mathbf{r}, \mathbf{v}; t)$ as

$$n_i = \int d\mathbf{v}\, f_i(\mathbf{v}), \tag{2.1}$$

$$\rho \mathbf{u} = \sum_i m_i n_i \mathbf{u}_i = \sum_i m_i \int d\mathbf{v}\, \mathbf{v} f_i(\mathbf{v}), \tag{2.2}$$

$$nT = p = \sum_i n_i T_i = \sum_i \frac{m_i}{d} \int d\mathbf{v}\, V^2 f_i(\mathbf{v}), \tag{2.3}$$

where $\mathbf{V} = \mathbf{v} - \mathbf{u}$ is the peculiar velocity, $n = \sum_i n_i$ is the total number density, $\rho = \sum_i \rho_i = \sum_i m_i n_i$ is the total mass density and p is the pressure. Furthermore, the second equality of equation (2.2) and the third equality of equation (2.3) define the flow velocity $\mathbf{u}_i$ and the partial kinetic temperature T_i for each species, respectively. In addition, in the dilute limit the pressure tensor P_i and the heat flux $\mathbf{q}_i$ associated with species i are given by

$$\mathsf{P}_i = m_i \int d\mathbf{v}\, \mathbf{V}\mathbf{V} f_i(\mathbf{v}), \qquad \mathbf{q}_i = \frac{m_i}{2} \int d\mathbf{v}\, V^2 \mathbf{V} f_i(\mathbf{v}). \tag{2.4}$$

In the low-density regime the distribution functions f_i obey a set of coupled nonlinear Boltzmann equations [24]:

$$(\partial_t + \mathbf{v} \cdot \nabla) f_i = \sum_j J_{ij}[\mathbf{v}|f_i, f_j], \tag{2.5}$$

where $J_{ij}[\mathbf{v}|f_i, f_j]$ denotes the inelastic Boltzmann operator that gives the rate of change of f_i due to collisions with particles of species j. It is given by

$$J_{ij}[\mathbf{v}_1|f_i, f_j] = \sigma_{ij}^{d-1} \int d\mathbf{v}_2 \int d\widehat{\boldsymbol{\sigma}}\, \Theta(\widehat{\boldsymbol{\sigma}} \cdot \mathbf{g}_{12})(\widehat{\boldsymbol{\sigma}} \cdot \mathbf{g}_{12})$$
$$\times \left[\alpha_{ij}^{-2} f_i(\mathbf{r}, \mathbf{v}_1', t) f_j(\mathbf{r}, \mathbf{v}_2', t) - f_i(\mathbf{r}, \mathbf{v}_1, t) f_j(\mathbf{r}, \mathbf{v}_2, t) \right]. \tag{2.6}$$

In equation (2.6), d is the dimensionality of the system, $\sigma_{ij} = (\sigma_i + \sigma_j)/2$, $\widehat{\boldsymbol{\sigma}}$ is a unit vector along the line of centers, Θ is the Heaviside step function and $\mathbf{g}_{12} = \mathbf{v}_1 - \mathbf{v}_2$ is the relative velocity. The primes on the velocities denote the initial values $\{\mathbf{v}_1', \mathbf{v}_2'\}$ that lead to $\{\mathbf{v}_1, \mathbf{v}_2\}$ following a binary (restituting) collision:

$$\mathbf{v}_1' = \mathbf{v}_1 - \mu_{ji}\left(1 + \alpha_{ij}^{-1}\right)(\widehat{\boldsymbol{\sigma}} \cdot \mathbf{g}_{12})\widehat{\boldsymbol{\sigma}}, \tag{2.7a}$$

$$\mathbf{v}_2' = \mathbf{v}_2 + \mu_{ij}\left(1 + \alpha_{ij}^{-1}\right)(\widehat{\boldsymbol{\sigma}} \cdot \mathbf{g}_{12})\widehat{\boldsymbol{\sigma}}, \tag{2.7b}$$

where $\mu_{ij} \equiv m_i/(m_i + m_j)$, so that $\mu_{ij} + \mu_{ji} = 1$.

However, due to the mathematical complexity of the Boltzmann equation, and in order to describe general nonequilibrium states, it is useful to replace the Boltzmann collision operator $J_{ij}[\mathbf{v}|f_i, f_j]$ with a more tractable *model* operator $K_{ij}[\mathbf{v}|f_i, f_j]$ that reproduces the collisional transfers of mass, momentum and energy of the true inelastic Boltzmann

operator, namely

$$\int d\mathbf{v} \begin{Bmatrix} 1 \\ \mathbf{v} \\ v^2 \end{Bmatrix} J_{ij}[\mathbf{v}|f_i, f_j] = \int d\mathbf{v} \begin{Bmatrix} 1 \\ \mathbf{v} \\ v^2 \end{Bmatrix} K_{ij}[\mathbf{v}|f_i, f_j]. \tag{2.8}$$

Extending the model proposed by Brey *et al* [43] for the monocomponent case and enforcing equation (2.8) in the Gaussian approximation, we have recently proposed the following model kinetic equation for inelastic mixtures [39]:

$$\partial_t f_i + \mathbf{v} \cdot \nabla f_i = -\sum_j \left\{ \frac{1 + \alpha_{ij}}{2} \nu_{ij} \left[f_i(\mathbf{v}) - f_{ij}(\mathbf{v}) \right] + \frac{\zeta_{ij}}{2} \frac{\partial}{\partial \mathbf{v}} \cdot \left[(\mathbf{v} - \mathbf{u}_i) f_i(\mathbf{v}) \right] \right\}, \tag{2.9}$$

where

$$\nu_{ij} = \frac{4\pi^{(d-1)/2}}{d\Gamma(d/2)} n_j \sigma_{ij}^{d-1} \left(\frac{2\widetilde{T}_i}{m_i} + \frac{2\widetilde{T}_j}{m_j} \right)^{1/2} \tag{2.10}$$

is a velocity-independent effective collision frequency of a particle of species i with particles of species j,

$$\zeta_{ij} = \frac{1}{2}\nu_{ij}\mu_{ji}^2 \left[1 + \frac{m_i\widetilde{T}_j}{m_j\widetilde{T}_i} + \frac{3}{2d}\frac{m_i}{\widetilde{T}_i}(\mathbf{u}_i - \mathbf{u}_j)^2 \right] (1 - \alpha_{ij}^2) \tag{2.11}$$

is the contribution to the cooling rate of species i due to the inelastic collisions with particles of species j and

$$f_{ij}(\mathbf{v}) = n_i \left(\frac{m_i}{2\pi T_{ij}} \right)^{d/2} \exp\left[-\frac{m_i}{2T_{ij}}(\mathbf{v} - \mathbf{u}_{ij})^2 \right] \tag{2.12}$$

is a reference distribution function. In the above equations

$$\widetilde{T}_i = \frac{m_i}{dn_i} \int d\mathbf{v}\,(\mathbf{v} - \mathbf{u}_i)^2 f_i = T_i - \frac{m_i}{d}(\mathbf{u}_i - \mathbf{u})^2, \tag{2.13}$$

$$\mathbf{u}_{ij} = \mu_{ij}\mathbf{u}_i + \mu_{ji}\mathbf{u}_j, \tag{2.14}$$

$$T_{ij} = \widetilde{T}_i + 2\mu_{ij}\mu_{ji} \left\{ \widetilde{T}_j - \widetilde{T}_i + \frac{(\mathbf{u}_i - \mathbf{u}_j)^2}{2d} \left[m_j + \frac{\widetilde{T}_j - \widetilde{T}_i}{\widetilde{T}_i/m_i + \widetilde{T}_j/m_j} \right] \right\}. \tag{2.15}$$

We now specialize to the problem analyzed in this paper, namely a binary mixture where one of the species ($i = 1$) is present in tracer concentration ($n_1/n_2 \to 0$). In this case, equations (2.2) and (2.3) imply that $\mathbf{u} = \mathbf{u}_2$ and $T = T_2$. In addition, the mixture is subjected to the steady Couette flow (see figure 1), so that the spatial dependence of all the quantities is limited to the y variable. In the tracer limit, the state of the excess component ($i = 2$) is not disturbed by the presence of the impurity and so equation (2.9) for $i = 2$ becomes

$$v_y \frac{\partial f_2}{\partial y} = -\nu_2(f_2 - f_{22}) + \frac{\zeta_{22}}{2}\frac{\partial}{\partial \mathbf{v}} \cdot \left[(\mathbf{v} - \mathbf{u}_2) f_2 \right], \tag{2.16}$$

where, according to equations (2.10)–(2.15), ν_2, ζ_{22} and f_{22} are given by

$$\nu_2 = \frac{1 + \alpha_{22}}{2}\nu_{22}, \qquad \nu_{22} = \frac{8\pi^{(d-1)/2}}{d\Gamma(d/2)}n_2\sigma_2^{d-1}\sqrt{\frac{T_2}{m_2}}, \tag{2.17}$$

$$\zeta_{22} = \frac{1 - \alpha_{22}^2}{4}\nu_{22} = \frac{1 - \alpha_{22}}{2}\nu_2, \tag{2.18}$$

$$f_{22}(\mathbf{v}) = n_2 \left(\frac{m_2}{2\pi T_2}\right)^{d/2} \exp\left[-\frac{m_2(\mathbf{v} - \mathbf{u}_2)^2}{2T_2}\right]. \tag{2.19}$$

Taking moments in equation (2.16), one gets the balance equations of momentum and energy in the steady state:

$$\frac{\partial P_{2,xy}}{\partial y} = \frac{\partial P_{2,yy}}{\partial y} = 0, \tag{2.20}$$

$$\frac{\partial q_{2,y}}{\partial y} + \frac{\partial u_{2,x}}{\partial y}P_{2,xy} = -\frac{d}{2}\zeta_{22}n_2 T_2. \tag{2.21}$$

Since the impurity only collides with particles of the host gas, equation (2.9) for $i = 1$ reduces to

$$v_y \frac{\partial f_1}{\partial y} = -\nu_1(f_1 - f_{12}) + \frac{\zeta_{12}}{2}\frac{\partial}{\partial \mathbf{v}} \cdot \left[(\mathbf{v} - \mathbf{u}_1)f_1\right], \tag{2.22}$$

where

$$\nu_1 = \frac{1 + \alpha_{12}}{2}\nu_{12}, \tag{2.23}$$

and ν_{12}, ζ_{12} and f_{12} are defined by equations (2.10)–(2.15) with $\widetilde{T}_2 = T_2 = T$. The kinetic equations (2.16) and (2.22) must be supplemented by appropriate boundary conditions representing the relative motion of the plates at $y = \pm L/2$.

The main advantage of the tracer limit is that f_2 obeys a closed (inelastic) kinetic equation (the same equation as the monocomponent granular gas). Once solved, the moments $n_2(y)$, $\mathbf{u}_2(y)$ and $T_2(y)$ can be inserted into equation (2.22) to get a closed equation for f_1. Despite the simplicity of the kinetic model with respect to the original Boltzmann equation, the search for an exact solution to the nonlinear Couette-flow problem is a formidable task. In the case of a monocomponent gas, an exact *hydrodynamic* solution was found in [37]. Of course, this solution holds for the kinetic equation (2.16) of the excess component. Based on this solution, in the next section we obtain an exact *hydrodynamic* solution for the kinetic equation (2.22) of the impurity.

3. Hydrodynamic solution beyond Navier–Stokes order

3.1. Excess component

As said before, an exact solution to (2.16) was found in [37]. Such a solution is characterized by the following hydrodynamic profiles:

$$p_2 = n_2 T_2 = \text{const}, \tag{3.1}$$

$$\frac{1}{\nu_2(y)}\frac{\partial}{\partial y}u_{2,x} = a = \text{const}, \tag{3.2}$$

$$\frac{1}{2m_2}\left[\frac{1}{\nu_2(y)}\frac{\partial}{\partial y}\right]^2 T_2 = -\gamma(a,\alpha_{22}) = \text{const}, \tag{3.3}$$

where $\gamma(a,\alpha_{22}) \geq 0$ is a dimensionless nonlinear function of the shear rate a and the coefficient of restitution α_{22}. This quantity (henceforth called the thermal curvature coefficient) characterizes the curvature of the temperature profile as a consequence of both the viscous heating and the collisional cooling. The form of the profiles (3.1)–(3.3) coincides with the profiles (1.4), (1.6) and (1.7) predicted by the NS description, except that the thermal curvature coefficient γ differs from its NS value and is determined consistently, as shown below. The solution to equations (3.2) and (3.3) is

$$u_{2,x}(s) = as, \qquad T_2(s) = T_2(0) + \epsilon s - m_2\gamma s^2, \tag{3.4}$$

where the scaled variable s is defined as

$$s(y) = \int_0^y \mathrm{d}y'\,\nu_2(y'), \tag{3.5}$$

and ϵ is an arbitrary constant that vanishes if the two wall temperatures are equal but is nonzero otherwise $(T_+ \neq T_-)$ [42].

For convenience, we refer the velocities of the particles to the Lagrangian frame moving with velocity $u_{2,x}(s)$. In this frame, equation (2.16) can be rewritten as

$$\left(1 - \frac{d}{2}\zeta_2^* + V_y\partial_s - aV_y\partial_{V_x} - \frac{1}{2}\zeta_2^*\mathbf{V}\cdot\partial_{\mathbf{V}}\right)f_2(s,\mathbf{V}) = f_{22}(s,\mathbf{V}), \tag{3.6}$$

where

$$\zeta_2^* = \frac{\zeta_{22}}{\nu_2} = \frac{1-\alpha_{22}}{2}, \tag{3.7}$$

and the derivative ∂_s is taken at constant $\mathbf{V} = \mathbf{v} - \mathbf{u}_2(s)$. Note that the dependence of the reference distribution f_{22} on both s and $\mathbf{V}$ is explicit. Taking this into account, the hydrodynamic solution to equation (3.6) is [37]

$$f_2(s,\mathbf{V}) = \int_0^\infty \mathrm{d}w\, \mathrm{e}^{-(1-(d/2)\zeta_2^*)w}\mathrm{e}^{-\tau(w,\zeta_2^*)V_y\partial_s}\mathrm{e}^{awV_y\partial_{V_x}}f_{22}(s,\mathrm{e}^{(1/2)\zeta_2^* w}\mathbf{V}), \tag{3.8}$$

where

$$\tau(w,\zeta_2^*) \equiv \frac{2}{\zeta_2^*}\left(\mathrm{e}^{(1/2)\zeta_2^* w} - 1\right). \tag{3.9}$$

The action of the operators $\mathrm{e}^{-\tau V_y\partial_s}$ and $\mathrm{e}^{awV_y\partial_{V_x}}$ on an arbitrary function $g(s,\mathbf{V})$ is

$$\mathrm{e}^{-\tau V_y\partial_s}g(s,\mathbf{V}) = g(s-\tau V_y,\mathbf{V}), \qquad \mathrm{e}^{awV_y\partial_{V_x}}g(s,V_x) = g(s,V_x+awV_y), \tag{3.10}$$

respectively. The solution (3.8) clearly adopts the form of a hydrodynamic or *normal* solution since its spatial dependence only occurs through a functional dependence on the hydrodynamic fields $n_2(s)$, $\mathbf{u}_2(s)$ and $T_2(s)$. This provides a neat example of the existence

of normal solutions beyond the NS domain. The solution (3.8) depends parametrically on the shear rate a, the coefficient of restitution α_{22} and the thermal curvature coefficient γ. However, only the two first parameters are independent since, as indicated by the notation in equation (3.3), γ is a nonlinear function of a and α_{22}. The parameter $\gamma(a, \alpha_{22})$ is determined by imposing the consistency conditions

$$\int \mathrm{d}\mathbf{v}\, \{1, \mathbf{V}, V^2\}(f_2 - f_{22}) = \{0, \mathbf{0}, 0\}. \tag{3.11}$$

While the first two conditions are identically satisfied, regardless of the value of γ, the third condition in (3.11) leads to the following implicit equation[1]:

$$d\frac{\zeta_2^*}{1 + \zeta_2^*} - \frac{2a^2}{(1 + \zeta_2^*)^3} = 2F_{1,0}(\gamma, \zeta_2^*) + dF_{0,0}(\gamma, \zeta_2^*) + a^2\left[2F_{1,2}(\gamma, \zeta_2^*) + F_{0,2}(\gamma, \zeta_2^*)\right]. \tag{3.12}$$

Here, we have introduced the mathematical functions

$$F_{0,m}(y, z) = \int_0^\infty \mathrm{d}w\, \mathrm{e}^{-(1+z)w} w^m \left[\sqrt{\pi}\theta(w, y, z)\mathrm{e}^{\theta^2(w,y,z)}\mathrm{erfc}\left(\theta(w, y, z)\right) - 1\right], \tag{3.13}$$

$$\begin{aligned}
F_{1,m}(y, z) &= y\frac{\partial}{\partial y}F_{0,m}(y, z) \\
&= -\tfrac{1}{2}\int_0^\infty \mathrm{d}w\, \mathrm{e}^{-(1+z)w} w^m \theta(w, y, z)\Big\{\sqrt{\pi}[1 + 2\theta^2(w, y, z)] \\
&\quad \times \mathrm{e}^{\theta^2(w,y,z)}\mathrm{erfc}(\theta(w, y, z)) - 2\theta(w, y, z)\Big\},
\end{aligned} \tag{3.14}$$

where $\mathrm{erfc}(x)$ is the complementary error function and

$$\theta(w, y, z) = \frac{1}{2\sqrt{2y}}\frac{z}{1 - \mathrm{e}^{-(1/2)zw}}. \tag{3.15}$$

The representation (3.12) exists only for $\gamma \geq 0$ or, equivalently, for $a \geq a_{\mathrm{th}}$, where, as discussed in section 1, the threshold value a_{th} of the shear rate corresponds to $\gamma = 0$. In this case, $F_{0,m}(0, \zeta_2^*) = F_{1,m}(0, \zeta_2^*) = 0$ (see the appendix) and so

$$a_{\mathrm{th}}^2 = \frac{d}{2}\zeta_2^*(1 + \zeta_2^*)^2. \tag{3.16}$$

In the case $a = a_{\mathrm{th}}$ the viscous heating is exactly balanced by collisional cooling. This state corresponds with the well-known simple shear flow (if $\epsilon = 0$ in (3.4)) but also to a non-uniform steady flow (for $\epsilon \neq 0$) that has been reported recently [42].

   Once the parameter γ is obtained from equation (3.12), the velocity distribution function is completely determined from equation (3.8). Its relevant moments provide the

---

[1] Note that, for convenience, the expressions for γ, the pressure tensor and the heat flux have been written in a representation slightly different from that of [37]. Of course, both representations are completely equivalent.

momentum and heat fluxes. The nonzero elements of the pressure tensor are given by [37]

$$\frac{P_{2,xx}}{p_2} = \frac{1}{1+\zeta_2^*} + 2\frac{a^2}{(1+\zeta_2^*)^3} + F_{0,0}(\gamma,\zeta_2^*) + a^2\left[F_{0,2}(\gamma,\zeta_2^*) + 2F_{1,2}(\gamma,\zeta_2^*)\right], \tag{3.17}$$

$$\frac{P_{2,yy}}{p_2} = \frac{1}{1+\zeta_2^*} + F_{0,0}(\gamma,\zeta_2^*) + 2F_{1,0}(\gamma,\zeta_2^*), \tag{3.18}$$

$$\frac{P_{2,zz}}{p_2} = \frac{1}{1+\zeta_2^*} + F_{0,0}(\gamma,\zeta_2^*), \tag{3.19}$$

$$\frac{P_{2,xy}}{p_2} = -a\left[\frac{1}{(1+\zeta_2^*)^2} + F_{0,1}(\gamma,\zeta_2^*) + 2F_{1,1}(\gamma,\zeta_2^*)\right]. \tag{3.20}$$

The requirement $[P_{2,xx} + P_{2,yy} + (d-2)P_{2,zz}]/p_2 = d$ is equivalent to the consistency condition (3.12). Equation (3.20) strongly differs from Newton's shearing law (see equation (1.5)) since the quantity enclosed by square brackets in equation (3.20) is a highly nonlinear function of the shear rate a through the thermal curvature coefficient γ. For instance, at $\alpha_{22} = 0.8$ and $a = 1$ the magnitude of $P_{2,xy}$ is about half its Newtonian value.

Next, we consider the heat flux components $q_{2,x}$ and $q_{2,y}$. The latter can be easily determined in terms of $P_{2,xy}$ making use of the energy balance equation (2.21), according to which $q_{2,y}$ is linear in s. Consequently, one gets

$$q_{2,y} = -\frac{p_2}{2m_2\nu_2\gamma}\left(a\frac{|P_{2,xy}|}{p_2} - \frac{d}{2}\zeta_2^*\right)\frac{\partial T_2}{\partial y}, \tag{3.21}$$

where we have taken into account that $\partial_s T_2$ is also linear in s (see equation (3.4)). Equation (3.21) can be seen as a generalized Fourier's law in the sense that $q_{2,y}$ is proportional to the thermal gradient with an effective thermal conductivity that is a nonlinear function of the shear rate. The evaluation of the component $q_{2,x}$ is much more involved. Multiplying both sides of equation (3.8) by $V^2 V_x$ and integrating over velocity, one gets [37]

$$q_{2,x} = \frac{p_2}{m_2\nu_2\sqrt{2\gamma}}a\left[G(\gamma,\zeta_2^*) + a^2 H(\gamma,\zeta_2^*)\right]\frac{\partial T_2}{\partial y}, \tag{3.22}$$

where we have called

$$G(y,z) = \int_0^\infty \mathrm{d}w\, \mathrm{e}^{-(1+(3/2)\zeta_2^*)w}w\left[\frac{d+1}{2}X(\theta(w,y,z)) + Y(\theta(w,y,z))\right], \tag{3.23}$$

$$H(y,z) = \int_0^\infty \mathrm{d}w\, \mathrm{e}^{-(1+(3/2)\zeta_2^*)w}w^3 Y(\theta(w,y,z)). \tag{3.24}$$

Here,

$$X(\theta) = \theta^2\left[\sqrt{\pi}(1+2\theta^2)\mathrm{e}^{\theta^2}\mathrm{erfc}(\theta) - 2\theta\right], \tag{3.25}$$

$$Y(\theta) = \theta^3\left[2(1+\theta^2) - \sqrt{\pi}\theta(3+2\theta^2)\mathrm{e}^{\theta^2}\mathrm{erfc}(\theta)\right]. \tag{3.26}$$

The existence of a component of the heat flux orthogonal to the thermal gradient and parallel to the flow direction goes beyond Fourier's law. In fact, $q_{2,x}$ is at least of order $a(\partial T_2/\partial y)$ and so equation (3.22) can be seen as a generalized Burnett effect.

3.2. Impurity particle

Once the hydrodynamic state of the excess component has been characterized, we next want to analyze the hydrodynamic state of the impurity particle.

First, some useful information can be extracted by taking moments in equation (2.22):

$$\frac{\partial P_{1,yy}}{\partial y} = 0, \tag{3.27}$$

$$\frac{\partial P_{1,xy}}{\partial y} = -\nu_1 \rho_1 \left(u_{1,x} - u_{12,x} \right), \tag{3.28}$$

$$\frac{\partial q_{1,y}}{\partial y} + \frac{\partial u_{2,x}}{\partial y} P_{1,xy} = -\nu_1 \left[\frac{d}{2} n_1 (T_1 - T_{12}) - \frac{\rho_1}{2} (\mathbf{u}_{12} - \mathbf{u}_2)^2 \right]$$
$$- \frac{d}{2} \zeta_{12} n_1 \left[T_1 - \frac{m_1}{d} (\mathbf{u}_1 - \mathbf{u}_2)^2 \right]. \tag{3.29}$$

Next, we guess (to be confirmed later) that the hydrodynamic state of the impurity is enslaved to that of the granular gas in the sense that

(i) there is no mutual diffusion, i.e. $\mathbf{u}_1(y) = \mathbf{u}_2(y)$,

(ii) the mole fraction $n_1(y)/n_2(y)$ is uniform, and

(iii) the temperature ratio $\chi \equiv T_1(y)/T_2(y)$ is also uniform.

The latter parameter χ must be a function of the mass and size ratios

$$\mu = \frac{m_1}{m_2}, \qquad \omega = \frac{\sigma_1}{\sigma_2}, \tag{3.30}$$

the reduced shear rate a, and the coefficients of restitution α_{22} and α_{12}. Of course, the temperature ratio is $\chi = 1$ when the impurity is mechanically equivalent to the gas particles ($\mu = \omega = 1$, $\alpha_{12} = \alpha_{22}$). Taking into account assumption (i), equations (3.28) and (3.29) become

$$\frac{\partial P_{1,xy}}{\partial y} = 0, \tag{3.31}$$

$$\partial_s q_{1,y} + a P_{1,xy} = -\frac{d}{2} n_1 T_1 \frac{\nu_1}{\nu_2} \left(1 - \frac{T_{12}}{T_1} + \frac{\zeta_{12}}{\nu_1} \right). \tag{3.32}$$

Furthermore, assumptions (ii) and (iii) imply that the product $n_1 T_1$ and the ratios T_{12}/T_1, ν_1/ν_2 and ζ_{12}/ν_1 are constant quantities. The three latter are given by

$$\frac{T_{12}}{T_1} = 1 + \frac{2\mu(1-\chi)}{(1+\mu)^2 \chi}, \tag{3.33}$$

$$\frac{\nu_1}{\nu_2} = \frac{1 + \alpha_{12}}{1 + \alpha_{22}} \left(\frac{1+\omega}{2} \right)^{d-1} \sqrt{\frac{\mu + \chi}{2\mu}}, \tag{3.34}$$

$$\widetilde{\zeta}_1 \equiv \frac{\zeta_{12}}{\nu_1} = \frac{\mu + \chi}{(1+\mu)^2 \chi} (1 - \alpha_{12}). \tag{3.35}$$

From a formal point of view, the kinetic equation (2.16) becomes equation (2.22) by making the changes $f_2 \to f_1$, $f_{22} \to f_{12}$, $\nu_2 \to \nu_1$ and $\zeta_{22} \to \zeta_{12}$. The formal change $f_{22} \to f_{12}$ implies the changes $n_2 \to n_1$, $m_2 \to m_1$ and $T_2 \to T_{12}$. It is then convenient to introduce the auxiliary quantities

$$\widetilde{a} = \frac{1}{\nu_1(y)} \frac{\partial}{\partial y} u_{2,x} = a \frac{\nu_2}{\nu_1}, \tag{3.36}$$

$$\widetilde{\gamma} = -\frac{1}{2m_1} \left[\frac{1}{\nu_1(y)} \frac{\partial}{\partial y} \right]^2 T_{12} = \left(\frac{\nu_2}{\nu_1} \right)^2 \frac{T_{12}}{T_1} \frac{\chi}{\mu} \gamma. \tag{3.37}$$

Equations (3.36) and (3.37), along with $n_1 T_{12} = \text{const}$, define the profiles of the fields characterizing the distribution function f_{12}.

The formal mapping described above allows us to easily get the moments of f_1 from comparison with those of f_2. In particular, the two first self-consistency conditions are verified, namely

$$\int \mathrm{d}\mathbf{v} \{1, \mathbf{V}\} (f_1 - f_{12}) = \{0, \mathbf{0}\}, \tag{3.38}$$

regardless of the values of γ and χ. The third self-consistency condition is

$$\frac{m_1}{d} \int \mathrm{d}\mathbf{v} \, V^2 (f_1 - f_{12}) = n_1 T_1 \left(1 - \frac{T_{12}}{T_1} \right). \tag{3.39}$$

This condition determines the temperature ratio χ. To evaluate the left-hand side of equation (3.39), it is convenient to obtain first the nonzero elements of the partial pressure tensor P_1. Taking into account equations (3.17)–(3.20), one gets

$$\frac{P_{1,xx}}{n_1 T_{12}} = \frac{1}{1 + \widetilde{\zeta}_1} + 2 \frac{\widetilde{a}^2}{(1 + \widetilde{\zeta}_1)^3} + F_{0,0}(\widetilde{\gamma}, \widetilde{\zeta}_1) + \widetilde{a}^2 \left[F_{0,2}(\widetilde{\gamma}, \widetilde{\zeta}_1) + 2F_{1,2}(\widetilde{\gamma}, \widetilde{\zeta}_1) \right], \tag{3.40}$$

$$\frac{P_{1,yy}}{n_1 T_{12}} = \frac{1}{1 + \widetilde{\zeta}_1} + F_{0,0}(\widetilde{\gamma}, \widetilde{\zeta}_1) + 2F_{1,0}(\widetilde{\gamma}, \widetilde{\zeta}_1), \tag{3.41}$$

$$\frac{P_{1,zz}}{n_1 T_{12}} = \frac{1}{1 + \widetilde{\zeta}_1} + F_{0,0}(\widetilde{\gamma}, \widetilde{\zeta}_1), \tag{3.42}$$

$$\frac{P_{1,xy}}{n_1 T_{12}} = -\frac{\widetilde{a}}{(1 + \widetilde{\zeta}_1)^2} - \widetilde{a} F_{0,1}(\widetilde{\gamma}, \widetilde{\zeta}_1) - 2\widetilde{a} F_{1,1}(\widetilde{\gamma}, \widetilde{\zeta}_1), \tag{3.43}$$

where the functions $F_{0,m}(y, z)$ and $F_{1,m}(y, z)$ are defined by equations (3.13) and (3.14), respectively. Condition (3.39) is equivalent to $P_{1,xx} + P_{1,yy} + (d-2)P_{1,zz} = dn_1 T_1$, yielding

$$d \left(\frac{T_1}{T_{12}} - \frac{1}{1 + \widetilde{\zeta}_1} \right) - \frac{2\widetilde{a}^2}{(1 + \widetilde{\zeta}_1)^3} = 2F_{1,0}(\widetilde{\gamma}, \widetilde{\zeta}_1) + dF_{0,0}(\widetilde{\gamma}, \widetilde{\zeta}_1) + \widetilde{a}^2 \left[2F_{1,2}(\widetilde{\gamma}, \widetilde{\zeta}_1) + F_{0,2}(\widetilde{\gamma}, \widetilde{\zeta}_1) \right]. \tag{3.44}$$

For given values of the reduced shear rate a and the mechanical parameters of the system (α_{22}, α_{12}, μ and ω), equation (3.44), complemented with equation (3.12) and the relations (3.33)–(3.37), becomes a nonlinear closed equation for the temperature ratio χ, which must be solved numerically. In the case of mechanically equivalent particles,

equation (3.44) yields $\chi = 1$ and is equivalent to equation (3.12). Insertion of this solution into equations (3.40)–(3.43) gives the elements of the pressure tensor P_1.

We consider now the heat flux associated with the impurity. According to equation (3.32), $q_{1,y}$ is linear in s. Since $\partial_s T_2$ is also linear in s (cf equation (3.4)), one can write

$$q_{1,y} = -\frac{n_1 T_1}{2 m_2 \nu_2 \gamma} \left[a \frac{|P_{1,xy}|}{n_1 T_1} - \frac{d}{2} \frac{\nu_1}{\nu_2} \left(1 - \frac{T_{12}}{T_1} + \widetilde{\zeta}_1 \right) \right] \frac{\partial T_2}{\partial y}. \tag{3.45}$$

To get the x component of the heat flux, we make use again of the formal mapping described above. Thus, from equation (3.22) we obtain

$$q_{1,x} = \frac{n_1 T_{12}}{m_1 \nu_1 \sqrt{2\widetilde{\gamma}}} \widetilde{a} \left[G(\widetilde{\gamma}, \widetilde{\zeta}_1) + \widetilde{a}^2 H(\widetilde{\gamma}, \widetilde{\zeta}_1) \right] \frac{\partial T_{12}}{\partial y}. \tag{3.46}$$

3.3. Generalized transport coefficients for the impurity particle

In order to characterize the momentum and heat transport associated with the impurity particle we introduce five generalized transport coefficients. The shear stress $P_{1,xy}$ defines a (dimensionless) nonlinear shear viscosity coefficient η_1 as

$$P_{1,xy} = -\eta_1 \frac{n_1 T_2}{\nu_1} \frac{\partial u_{2,x}}{\partial y}. \tag{3.47}$$

The anisotropy of the normal stresses can be measured through the viscometric coefficients N_1 and M_1:

$$\frac{P_{1,xx} - P_{1,yy}}{n_1 T_1} = N_1, \qquad \frac{P_{1,zz} - P_{1,yy}}{n_1 T_1} = M_1. \tag{3.48}$$

The heat flux defines a generalized thermal conductivity coefficient λ_1 and a cross-coefficient ϕ_1 as

$$q_{1,y} = -\lambda_1 \frac{d+2}{2} \frac{n_1 T_2}{m_1 \nu_1} \frac{\partial T_2}{\partial y}, \qquad q_{1,x} = \phi_1 \frac{d+2}{2} \frac{n_1 T_2}{m_1 \nu_1} \frac{\partial T_2}{\partial y}. \tag{3.49}$$

From equations (3.40)–(3.43), (3.45) and (3.46) it is possible to identify the expressions for these five generalized transport coefficients. They are given by

$$\eta_1 = \frac{T_{12}}{T_1} \chi \left[\frac{1}{(1 + \widetilde{\zeta}_1)^2} + F_{0,1}(\widetilde{\gamma}, \widetilde{\zeta}_1) + 2 F_{1,1}(\widetilde{\gamma}, \widetilde{\zeta}_1) \right], \tag{3.50}$$

$$N_1 = \frac{T_{12}}{T_1} \left\{ 2 \frac{\widetilde{a}^2}{(1 + \widetilde{\zeta}_1)^3} + \widetilde{a}^2 \left[F_{0,2}(\widetilde{\gamma}, \widetilde{\zeta}_1) + 2 F_{1,2}(\widetilde{\gamma}, \widetilde{\zeta}_1) \right] - 2 F_{1,0}(\widetilde{\gamma}, \widetilde{\zeta}_1) \right\}, \tag{3.51}$$

$$M_1 = -2 \frac{T_{12}}{T_1} F_{1,0}(\widetilde{\gamma}, \widetilde{\zeta}_1), \tag{3.52}$$

$$\lambda_1 = \frac{1}{d+2} \frac{T_{12}}{T_1} \frac{\chi^2}{\widetilde{\gamma}} \left[\eta_1 \widetilde{a}^2 - \frac{d}{2} \left(1 - \frac{T_{12}}{T_1} + \widetilde{\zeta}_1 \right) \right], \tag{3.53}$$

$$\phi_1 = \frac{2}{d+2} \left(\frac{T_{12}}{T_1} \right)^2 \frac{\chi^2}{\sqrt{2\widetilde{\gamma}}} \widetilde{a} \left[G(\widetilde{\gamma}, \widetilde{\zeta}_1) + \widetilde{a}^2 H(\widetilde{\gamma}, \widetilde{\zeta}_1) \right]. \tag{3.54}$$

Their expressions in the limit $a \to a_{\text{th}}$ are explicitly given in the appendix.

4. Monte Carlo simulations

As said before, the exact solution to the kinetic equation (2.22) derived in section 3 defines a normal or hydrodynamic solution where its spatial dependence only occurs through the hydrodynamic fields (n_1, n_2, $\mathbf{u}_2$ and T_2) and their gradients. This solution is free from boundary-layer effects and formally corresponds to idealized boundary conditions of infinitely cold walls ($T_w \to 0$). For more details the reader is referred to appendix B of [37]. The important point is whether or not this exact solution actually describes the steady state reached by the system, in the bulk domain, when subject to realistic boundary conditions and for arbitrary initial conditions. To confirm this expectation, one needs to solve numerically the set of time-dependent kinetic equations

$$\partial_t f_i + v_y \frac{\partial f_i}{\partial y} = -\nu_i(f_i - f_{i2}) + \frac{\zeta_{i2}}{2} \frac{\partial}{\partial \mathbf{v}} \cdot (\mathbf{v} - \mathbf{u}_i) f_i \qquad i = 1, 2. \tag{4.1}$$

These equations are solved with boundary conditions at $y = \pm L/2$ compatible with the wall values $\pm U/2$ and T_w and starting from an arbitrary initial condition. Specifically, we have considered Maxwellian diffuse boundary conditions [37, 44] and an initial distribution of total equilibrium. The latter choice does not imply a loss of generality in the base steady states that are achieved in the system and only affects the transient evolution. Both species are let to simultaneously evolve from the initial state. It is also to be noticed that in the numerical solution of equation (4.1), there is no a priori assumption of equal flow velocities for the two components, i.e. eventual steady-state solutions with $\mathbf{u}_1 \neq \mathbf{u}_2$ are left to occur. However, as we will show, this actually never happens and all the steady states found are consistent with $\mathbf{u}_1 = \mathbf{u}_2$ (absence of diffusion).

In this paper we have employed a direct simulation Monte Carlo (DSMC) method [45, 46] to numerically solve the kinetic equations (4.1) in the three-dimensional case. The DSMC method has been extensively used to solve kinetic equations like the Boltzmann and BGK equations and it has proven to accurately describe transport phenomena in elastic gases and has also successfully been extended to flows in granular gases. In the DSMC method two steps are taken every time interval δt: the free streaming step, during which a particle with velocity $\mathbf{v}$ is drifted by $\mathbf{v} \delta t$ and the boundary conditions are applied to those particles leaving the system, and the collision step, in which $\nu_i \delta t$ collision pairs are randomly selected among neighbor particles, ν_i being the characteristic collision frequency in the kinetic equation. Our method differs from the elastic case in the addition, in the free streaming step, of the drag term which mimics the inelasticity in the collisions.

The distributions f_i are represented by $\mathcal{N}_i$ particles with velocities $\{\mathbf{v}_k\}$ and positions $\{y_k\}$, $k = 1, \ldots, \mathcal{N}_i$. The system is split into $\mathcal{M}$ layers $I = 1, \ldots, \mathcal{M}$ of width $\delta y = L/\mathcal{M}$. The particles with positions belonging in layer I define the densities $n_{i,I}$, the flow velocities $\mathbf{u}_{i,I}$ and the temperatures $T_{i,I}$ of that layer. From those quantities one can evaluate $\nu_{i,I}$ and $\zeta_{i2,I}$. The free streaming and the collision steps are briefly described below.

4.1. Free streaming

In the free streaming step the positions and velocities for both components are updated with the following rules:

$$\begin{aligned} y_k &\to y_k + v_{k,y} \delta t, \\ \mathbf{v}_k &\to \mathbf{u}_{i,I} + e^{-\zeta_{i2,I}\delta t/2} \left(\mathbf{v}_k - \mathbf{u}_{i,I} \right), \end{aligned} \tag{4.2}$$

where I is the layer the particle k belongs in. The spatial and velocity updates (4.2) are valid as long as the particle does not leave the system, i.e. $|y_k + v_{k,y}\delta t| < L/2$. Otherwise, the particle is reentered by applying thermal boundary conditions. If the particle 'crosses' a wall, then

$$\mathbf{v}_k \rightarrow \pm(U/2)\widehat{\mathbf{x}} + \mathbf{w}_k, \tag{4.3}$$

where the velocity components $w_{k,x}, w_{k,z}$ are randomly picked from Maxwell distribution functions (at a temperature T_w) whereas $w_{k,y} = \mp \upsilon$ (upper and lower signs for top and bottom wall collision, respectively) with $\upsilon > 0$ being a random velocity sampled from the Rayleigh probability distribution

$$P_i(\boldsymbol{\upsilon}) = \frac{m_i \upsilon}{T_w} e^{-m_i \upsilon^2/2T_w}. \tag{4.4}$$

The new position after wall collision is

$$y_i \rightarrow \pm L/2 + w_{k,y}\left(\delta t - \frac{\pm L/2 - y_k}{v_{k,y}}\right). \tag{4.5}$$

4.2. Collision step

For each layer I a number $\nu_{i,I}\delta t$ of particles is randomly selected among those belonging in the layer. Then the velocity $\mathbf{v}_k$ of each one of those particles is replaced by

$$\mathbf{v}_k \rightarrow \mathbf{u}_{i,I} + \mathbf{V}_k, \tag{4.6}$$

where $\mathbf{V}_k$ is a random velocity sampled from a Maxwell probability distribution, with temperatures T_{12} and T_2 for species $i = 1$ and $i = 2$, respectively.

4.3. Time and length scales and simulation technical facts

In the simulations, the quantities are reduced using $\overline{\ell}$ and $\overline{\tau}$ as length and time units, respectively, where

$$\overline{\ell} = \frac{3}{4(1+\alpha_{22})}\frac{1}{\sqrt{2\pi}\overline{n}_2\sigma_2^2}, \qquad \overline{\tau} = \frac{\overline{\ell}}{v_0}, \tag{4.7}$$

$\overline{n}_2$ and $v_0 = \sqrt{2T_w/m_2}$ being the average density of the gas particles and a reference thermal velocity, respectively.

Since the aim of DSMC simulations is to solve a kinetic equation, it must be able to describe the dynamical processes occurring in the system at a microscopic level [45]. This means that the width layer δy must be small compared to the typical microscopic length scale, determined by the mean free path ℓ_i. Similarly, the timestep δt must be small compared to the inverse of the collision frequency, ν_i^{-1}. Also, for obtaining an ergodic simulation, the number of simulated particles N_i must be sufficiently large. We therefore have performed simulations, for both species, with $N_i = 2 \times 10^6$ particles, $\delta y = 2 \times 10^{-2}\overline{\ell}$ and $\delta t = 3 \times 10^{-3}\overline{\tau}$. In order to probe a nonlinear Couette flow with $\gamma > 0$ ($a > a_{th}$), we have taken a wall velocity difference $U = 10v_0$ and a system size typically in the range $L \approx 2$–$20\overline{\ell}$, which produces sufficiently large values of a.

Taking into account that the relation between microscopic over hydrodynamic scales is given by the Knudsen number Kn, the bin δy_h we pick for measurements of the

hydrodynamic profiles, including transport coefficients, is of the order of $\delta y_{\mathrm{h}} = 0.2\mathrm{Kn}^{-1}\ell_i$ (note that, in our system, the reduced local shear rate a is the reference measure for the Knudsen number). This means that the measurements of the hydrodynamic properties are performed over sets of microscopic cells, i.e. an average over microscopic cells is taken for each set (macroscopic cell). In this way, the fluctuations of macroscopic magnitudes, typical in DSMC simulations, are greatly reduced and profiles are smoothed with no loss of resolution at a hydrodynamic scale. Prior to averaging over sets of cells, the hydrodynamic quantities and fluxes are obtained for each cell by using the expressions that may be found in [44].

As already explained in sections 1 and 3, the reduced shear rate a and the thermal curvature coefficient γ are fundamental quantities in the problem. We measured these quantities by fitting the velocity and temperature profiles from the simulations to fourth-degree polynomials and extracting from these fits the derivatives appearing in expressions (3.2) and (3.3).

An important point in DSMC simulations is the quality of the random number generator. We used for this purpose random generators from Intel MKL 9.1 [47], whose performance has been rigorously examined in technical tests. The DSMC code was written in the C language and compiled with an Intel C++ 10.0 compiler and run on 64-bit Linux machines.

5. Results

5.1. Enslaving of the impurity

The DSMC simulations described in section 4 show that the steady state reached by the system is in agreement with the bulk profiles assumed in the hydrodynamic solution worked out in section 3, i.e. the pressure p_2, the local shear rate a and the local thermal curvature γ are practically uniform. Moreover, the impurity properties are enslaved to those of the gas particles, namely the system evolves to $\mathbf{u}_1 = \mathbf{u}_2$, $n_1/n_2 = \mathrm{const}$ and $T_1/T_2 = \mathrm{const}$, in agreement with assumptions (i)–(iii) listed below equation (3.29). As an illustration, figure 3 shows simulation data of the pressure and velocity profiles for both the impurity and the gas particles at $t \approx \overline{\tau}$ and $t \approx 10^3\overline{\tau}$.

5.2. Thermal curvature coefficient

In the remainder of this section we compare the theoretical results derived in section 3 for $d = 3$ with the data obtained from our DSMC simulations. Before considering properties associated with the impurity, we first compare the shear rate dependence of the thermal curvature coefficient γ. Figure 4 displays γ versus a^2 for three values of the coefficient of restitution α_{22}: $\alpha_{22} = 1$ (elastic case), $\alpha_{22} = 0.9$ (moderately inelastic case) and $\alpha_{22} = 0.8$ (quite inelastic case). It is observed that the theory compares well with the simulation results for the three values of α_{22} considered, even for strongly sheared gases. This confirms the reliability of a (non-Newtonian) hydrodynamic description for granular gases in the bulk domain and beyond the quasi-elastic limit, at least within the framework of the model kinetic equations used. It is apparent from figure 4 that, at a given value of the reduced shear rate a, the value of γ decreases with increasing dissipation. This can be qualitatively understood by the tendency of the collisional cooling to produce a
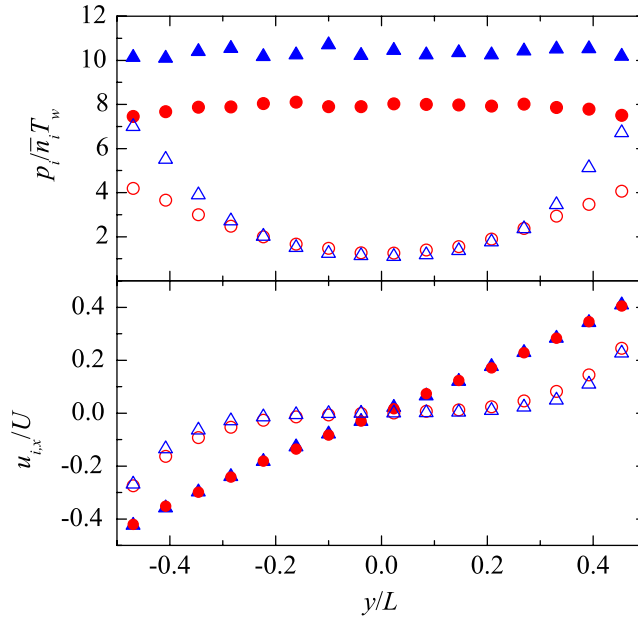
Figure 3. Pressure and flow velocity profiles for the impurity (triangles) and the gas particles (circles) at $t \approx \overline{\tau}$ (open symbols) and $t \approx 10^3 \overline{\tau}$ (filled symbols). The system corresponds to $\alpha_{12} = \alpha_{22} = 0.9$, $m_1/m_2 = 2$, $\sigma_1/\sigma_2 = 1$, $L = 3.25\overline{\ell}$ and $U = 10v_0$. At short times, the hydrostatic pressures p_i are not constant and the flow velocities $\mathbf{u}_i$ are not equal, but the simulation quickly evolves to $p_1 = \mathrm{const}$, $p_2 = \mathrm{const}$ and $\mathbf{u}_1 = \mathbf{u}_2$, just like in the theoretical solution. We observed analogous evolution in all simulations we performed, for a wide range of parameter values.

concave temperature profile, while the viscous heating tends to produce a convex profile. In fact, both tendencies cancel each other at the threshold shear rate a_{th}, where $\gamma = 0$. The corresponding values for $\alpha_{22} = 0.9$ and $\alpha_{22} = 0.8$, are $a_{\mathrm{th}} = 0.29$ and $a_{\mathrm{th}} = 0.43$, respectively. As noted above, our analytical solution is not mathematically well defined for negative values of γ (i.e. $a < a_{\mathrm{th}}$, shaded region in figure 2). This restriction obviously does not apply to the simulations, which can reach states with $\gamma < 0$. These states also include those in the absence of shearing ($a = 0$). States with $a = 0$ are interesting and some cases have been studied in the framework of the NS description and/or in the quasi-elastic limit [48].

5.3. Temperature ratio

Let us study now the main properties characterizing the hydrodynamic state of the impurity. The parameter space of the problem is made of four (dimensionless) material quantities (the mass ratio $\mu = m_1/m_2$, the size ratio $\omega = \sigma_1/\sigma_2$ and the coefficients of restitution α_{12} and α_{22}) plus the reduced shear rate a. For the sake of illustration, we will assume a common coefficient of restitution $\alpha_{12} = \alpha_{22} = \alpha$ and a common size ($\omega = 1$), so that the parameter space becomes three-dimensional. Furthermore, we focus on three values of μ ($\mu = 2$, 1 and 0.5) and three values of α ($\alpha = 1$, 0.9 and 0.8), so that we consider nine different systems. For each one, we analyze the dependence of the properties
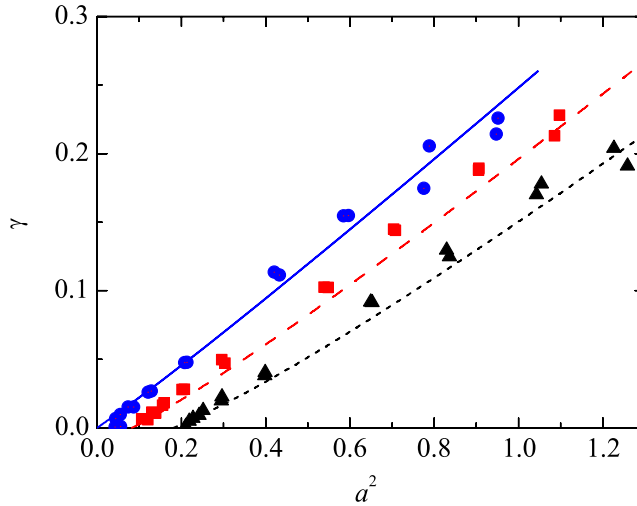
Figure 4. Shear rate dependence of the parameter γ measuring the curvature of the temperature profile (see equation (3.3)) for $\alpha_{22} = 1$ (solid line and circles), $\alpha_{22} = 0.9$ (dashed line and squares) and $\alpha_{22} = 0.8$ (dotted line and triangles). The symbols represent the simulation results, while the lines are the theoretical predictions given by equation (3.12).

of the impurity on the shear rate. Note that, since $\omega = 1$ and $\alpha_{12} = \alpha_{22}$, in the case $\mu = 1$ the impurity is mechanically equivalent to the gas particles.

First, the breakdown of energy equipartition, as measured by the temperature ratio $\chi = T_1/T_2$, is plotted in figure 5. A good agreement between theory and simulations is observed. The lack of energy equipartition is expected because of two reasons. On the one hand, the state of the system is far from equilibrium due to the shearing and thus $T_1 \neq T_2$, even in the elastic case ($\alpha = 1$) [49, 50]. On the other hand, even in the homogeneous cooling state, the inelasticity drives the system out of equilibrium and, consequently, $T_1 \neq T_2$ [10]. We see from figure 5 that the impurity has a higher (lower) granular temperature than the gas if it is heavier (lighter) than a gas particle. This agrees with the general trend observed in experiments [22, 23]. Figure 5 also shows that, for a given value of α, the deviation of the temperature ratio from unity increases as the shear rate increases. Similarly, at a given value of a, the deviation $\chi - 1$ becomes more important with increasing dissipation.

5.4. Generalized transport coefficients

Next, we explore the momentum and heat transport of the impurity, as measured by the rheological quantities η_1, N_1, M_1, λ_1 and ϕ_1 defined by equations (3.47)–(3.49). Figures 6–8 display the three transport coefficients associated with the pressure tensor. As in the case of χ, the agreement between the theoretical predictions and the simulation results is very good. It is apparent that, regardless of the value of α, shear thinning effects are present, i.e. the nonlinear shear viscosity η_1 decreases with increasing shear rate. Regarding the influence of the mass ratio, we observe that, for fixed values of α and a, η_1 increases as the mass ratio increases. The influence of dissipation on η_1 is smaller than that of μ. In any case, although hardly apparent in figure 6, the value of η_1 increases as α decreases at
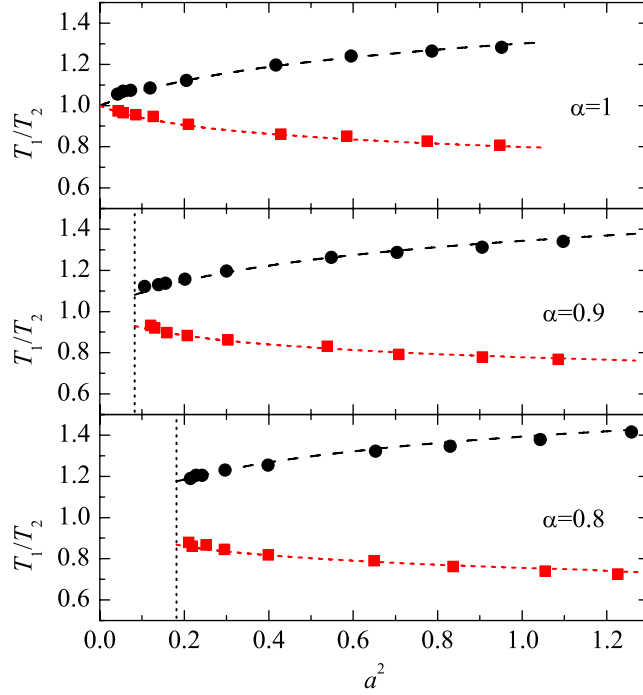
Figure 5. Shear rate dependence of the temperature ratio $\chi \equiv T_1/T_2$ in the case of an impurity particle with $\omega \equiv \sigma_1/\sigma_2 = 1$, $\alpha_{11} = \alpha_{22} = \alpha$, $\mu \equiv m_1/m_2 = 2$ (dashed lines and circles) and $\mu \equiv m_1/m_2 = 1/2$ (dotted lines and squares). The symbols represent the simulation results, while the lines are the theoretical predictions given by equation (3.44). The top, middle and bottom panels correspond to $\alpha = 1$, $\alpha = 0.9$ and $\alpha = 0.8$, respectively. The dotted vertical lines indicate the location of the threshold value $a_{\rm th}^2(\alpha)$.

given μ and a. It is interesting to note that the ratio η_1/χ is practically independent of μ, although it exhibits a weak dependence on α.

The viscometric coefficients N_1 and M_1, which measure normal stress differences, are plotted in figures 7 and 8, respectively. The shearing produces a strong anisotropy in the normal stresses: $P_{1,xx} > n_1 T_1 > P_{1,zz} > P_{1,yy}$. As expected, this anisotropy increases with the shear rate. While, for given a and α, the coefficient N_1 increases as the impurity becomes heavier, the opposite happens with the coefficient M_1. With respect to the influence of α, it turns out that it is practically negligible in the case of N_1, while M_1 decreases significantly as the system becomes more inelastic.

Finally, the two transport coefficients λ_1 and ϕ_1 measuring the heat flux are plotted in figures 9 and 10, respectively. These coefficients are quite difficult to measure in the simulations near the threshold shear rate $a_{\rm th}$, since there the thermal gradient is very small. This explains the scatter of the simulation data near $a^2 = a_{\rm th}^2$. Again, theory compares quite well with simulations. This is rather satisfactory especially in the case of ϕ_1 since this cross-coefficient measures complex coupling effects between the velocity and temperature gradients, which are absent in the NS regime. Figure 9 shows that, analogously to what happens with η_1, the generalized thermal conductivity λ_1 decreases with increasing shear rate. In contrast, the cross-coefficient ϕ_1 has a non-monotonic dependence for small
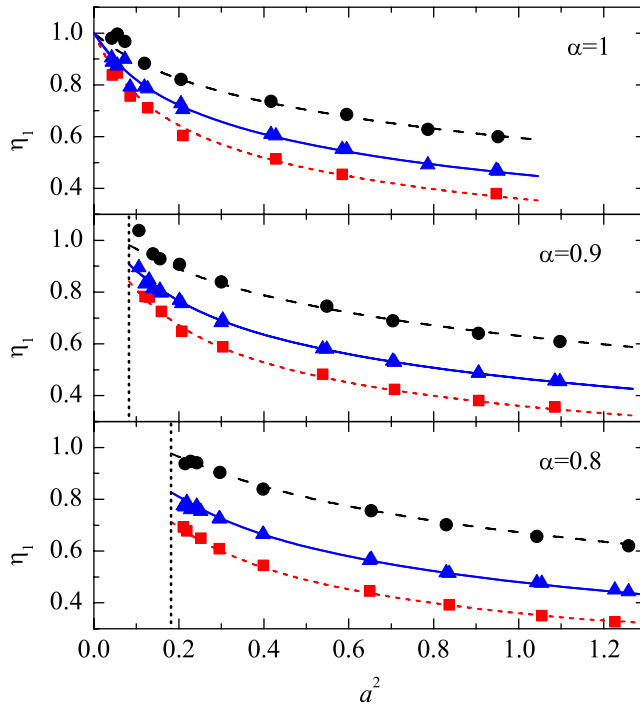
Figure 6. Shear rate dependence of the nonlinear shear viscosity coefficient η_1 (see equation (3.47)) associated with an impurity particle with $\omega \equiv \sigma_1/\sigma_2 = 1$, $\alpha_{11} = \alpha_{22} = \alpha$, $\mu \equiv m_1/m_2 = 2$ (dashed lines and circles), $\mu \equiv m_1/m_2 = 1$ (solid lines and triangles) and $\mu \equiv m_1/m_2 = 1/2$ (dotted lines and squares). The symbols represent the simulation results, while the lines are the theoretical predictions given by equation (3.50). The top, middle and bottom panels correspond to $\alpha = 1$, $\alpha = 0.9$ and $\alpha = 0.8$, respectively. The dotted vertical lines indicate the location of the threshold value $a_{th}^2(\alpha)$.

inelasticities. In agreement with the behavior found for η_1 and N_1, both coefficients λ_1 and ϕ_1 decrease as the mass of the impurity decreases, at given values of a and α. As for the influence of α, the results show that λ_1 and ϕ_1 increase with increasing dissipation, this effect being more important for a heavy impurity than for a light impurity. We have observed that the influence of the mass ratio on λ_1 and ϕ_1 is significantly inhibited when one considers the ratios λ_1/χ^2 and ϕ_1/χ^2, especially in the former case. A remarkable counter-intuitive feature is that the coefficient ϕ_1 can turn out to be larger than λ_1 for sufficiently large shear rate. This effect is more notorious as the system becomes more inelastic and/or the impurity becomes heavier. In fact, in the cases $\mu = 1$ and 2 with $\alpha = 0.8$, one has $\phi_1 > \lambda_1$ for any shear rate larger than a_{th}. Taking into account the definitions (3.49), the situation $\phi_1 > \lambda_1$ implies that $|q_x| > |q_y|$, i.e. the shearing induces a heat flux with a component orthogonal to the thermal gradient that is larger than the component parallel to the gradient.

5.5. Preliminary DSMC results from the true Boltzmann equation

Thus far we have shown that the numerical solutions of the model kinetic equations (4.1) with realistic boundary conditions support the steady-state hydrodynamic solution
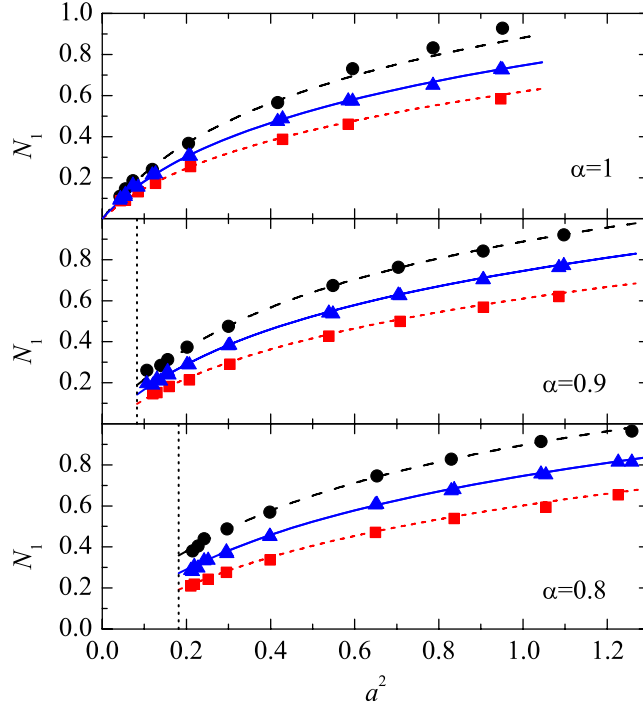
Figure 7. Shear rate dependence of the reduced normal stress difference N_1 (see equation (3.48)) associated with an impurity particle with $\omega \equiv \sigma_1/\sigma_2 = 1$, $\alpha_{11} = \alpha_{22} = \alpha$, $\mu \equiv m_1/m_2 = 2$ (dashed lines and circles), $\mu \equiv m_1/m_2 = 1$ (solid lines and triangles) and $\mu \equiv m_1/m_2 = 1/2$ (dotted lines and squares). The symbols represent the simulation results, while the lines are the theoretical predictions given by equation (3.51). The top, middle and bottom panels correspond to $\alpha = 1$, $\alpha = 0.9$ and $\alpha = 0.8$, respectively. The dotted vertical lines indicate the location of the threshold value $a_{\text{th}}^2(\alpha)$.

derived in this paper for the same model beyond the small Knudsen number limit. However, the important question is whether or not such a generalized hydrodynamic description is supported by the more fundamental Boltzmann equation. Comparison between DSMC simulations of the Boltzmann equation and the hydrodynamic solution of the kinetic model shows that the answer is affirmative in the case of a monocomponent granular gas [37].

When an impurity particle is embedded in the host granular gas, the crucial point of the hydrodynamic solution worked out in section 3 is the enslaving of the hydrodynamic fields of the impurity to those of the bath, as expressed by assumptions (i)–(iii) below equation (3.29). We have performed preliminary DSMC simulations of the Boltzmann equation for the host gas and the coupled Boltzmann–Lorentz equation for the impurity particle and have observed that properties (i)–(iii) are indeed satisfied in the steady state and in the bulk domain. As an illustrative example, figure 11 shows the pressure and velocity profiles, as obtained from DSMC simulations of the Boltzmann equation, for a system similar to that of figure 3 but with a larger separation between the plates. Again, in the steady state (and also practically during the transient regime) one has $\mathbf{u}_1 = \mathbf{u}_2$. Moreover, both p_1 and p_2 are practically constant in the bulk region. As in figure 3,
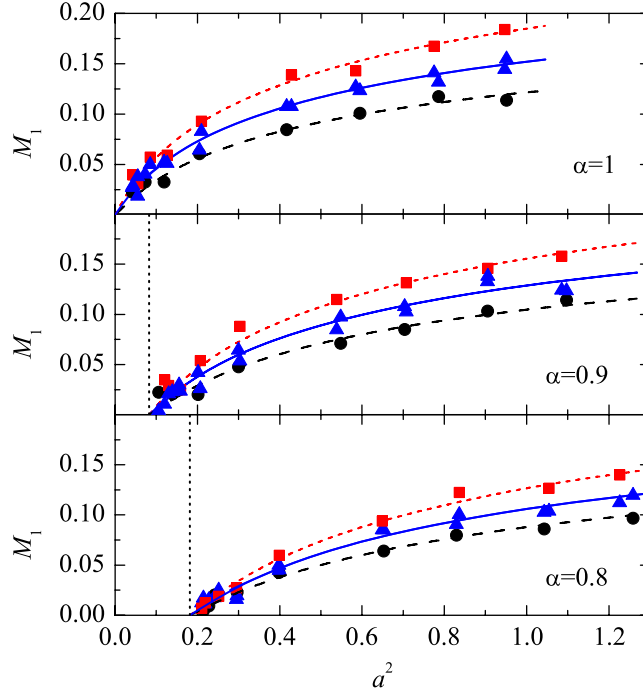
Figure 8. Shear rate dependence of the reduced normal stress difference M_1 (see equation (3.48)) associated with an impurity particle with $\omega \equiv \sigma_1/\sigma_2 = 1$, $\alpha_{11} = \alpha_{22} = \alpha$, $\mu \equiv m_1/m_2 = 2$ (dashed lines and circles), $\mu \equiv m_1/m_2 = 1$ (solid lines and triangles) and $\mu \equiv m_1/m_2 = 1/2$ (dotted lines and squares). The symbols represent the simulation results, while the lines are the theoretical predictions given by equation (3.52). The top, middle and bottom panels correspond to $\alpha = 1$, $\alpha = 0.9$ and $\alpha = 0.8$, respectively. The dotted vertical lines indicate the location of the threshold value $a_{\text{th}}^2(\alpha)$.

$p_1/\overline{n}_1 > p_2/\overline{n}_2$, but this effect is smaller than in figure 3 because now L is larger and so the shear rate a is smaller. Moreover, as exemplified by figures 3 and 11, we have observed that the boundary effects are more important in the case of the Boltzmann description than in that of the kinetic model. A more exhaustive study, including the temperature ratio and the generalized transport coefficients, is ongoing and will be published elsewhere [51].

6. Conclusions

In this paper we have analyzed the transport properties of impurities immersed in a granular gas under nonlinear steady planar Couette flow. We have focused on situations where the shear rate is large enough as to make the viscous heating term prevail over the inelastic cooling term in the energy balance equation. In these conditions the NS description is, in general, inadequate, as illustrated by figure 2, and so a more fundamental kinetic theory is needed. Due to the mathematical complexity of the Boltzmann equation, here we have used a kinetic model for granular mixtures recently proposed by the authors [39]. Our approach differs from a recent work [38] on a bidisperse granular fluid under Couette flow, where a continuum description is used. In addition, the present
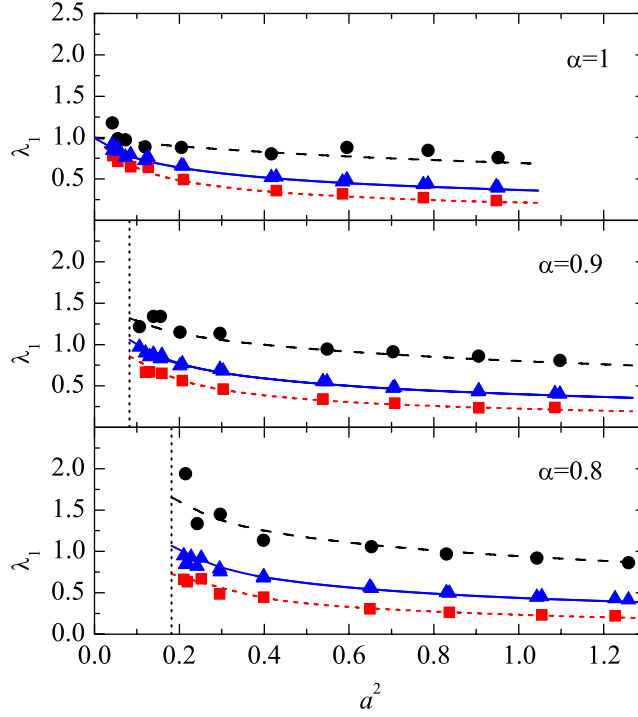
Figure 9. Shear rate dependence of the nonlinear thermal conductivity coefficient λ_1 (see equation (3.49)) associated with an impurity particle with $\omega \equiv \sigma_1/\sigma_2 = 1$, $\alpha_{11} = \alpha_{22} = \alpha$, $\mu \equiv m_1/m_2 = 2$ (dashed lines and circles), $\mu \equiv m_1/m_2 = 1$ (solid lines and triangles) and $\mu \equiv m_1/m_2 = 1/2$ (dotted lines and squares). The symbols represent the simulation results, while the lines are the theoretical predictions given by equation (3.53). The top, middle and bottom panels correspond to $\alpha = 1$, $\alpha = 0.9$ and $\alpha = 0.8$, respectively. The dotted vertical lines indicate the location of the threshold value $a_{\mathrm{th}}^2(\alpha)$.

work extends to inelastic collisions a previous study [49] carried out for ordinary gaseous mixtures.

Two different and complementary routes have been considered. First, an exact *hydrodynamic* (or 'normal') solution for the steady state has been found. This solution applies for arbitrarily large shear rates a (larger than the threshold value a_{th} corresponding to the simple shear flow) and arbitrary values of the parameters of the system (coefficients of restitution, masses and sizes). Progress has been made taking advantage of a formal mapping between the kinetic equation for the gas particles (whose exact hydrodynamic solution was found in [37]) and the kinetic equation for the impurity. This formal mapping is possible once it is guessed that the hydrodynamic profiles of the impurity are enslaved to those of the gas particles, i.e. n_1/n_2 and T_1/T_2 are uniform and $\mathbf{u}_1 = \mathbf{u}_2$ (no diffusion). Second, we have solved the set of two coupled kinetic equations by means of a DSMC method [45], with realistic boundary conditions. The numerical solution shows, in the context of our kinetic model description, the validity of the assumptions we make in the calculation of the theoretical solution. Furthermore, we have not found ranges of parameter values where these assumptions are not accurately fulfilled in the bulk of the fluid. Thus, an important corollary of this work is that, under Couette flow and for our
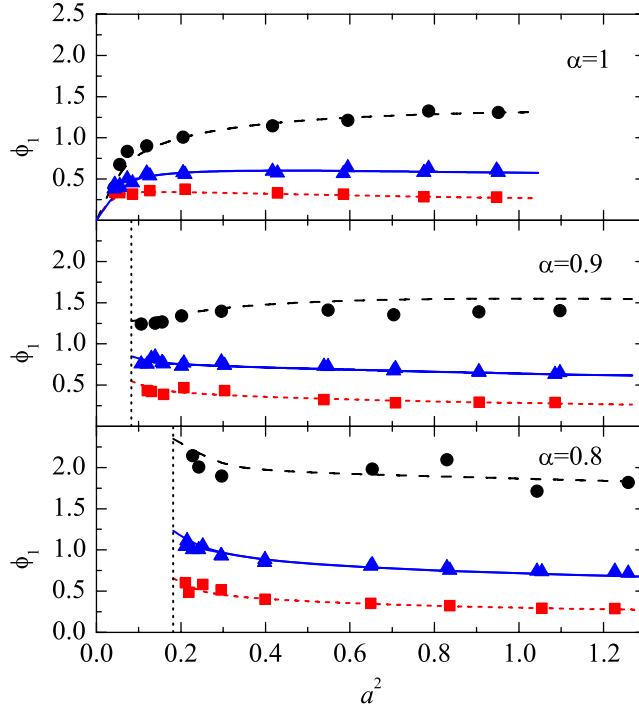
Figure 10. Shear rate dependence of the cross-coefficient ϕ_1 (see equation (3.49)) associated with an impurity particle with $\omega \equiv \sigma_1/\sigma_2 = 1$, $\alpha_{11} = \alpha_{22} = \alpha$, $\mu \equiv m_1/m_2 = 2$ (dashed lines and circles), $\mu \equiv m_1/m_2 = 1$ (solid lines and triangles) and $\mu \equiv m_1/m_2 = 1/2$ (dotted lines and squares). The symbols represent the simulation results, while the lines are the theoretical predictions given by equation (3.54). The top, middle and bottom panels correspond to $\alpha = 1$, $\alpha = 0.9$ and $\alpha = 0.8$, respectively. The dotted vertical lines indicate the location of the threshold value $a_{\mathrm{th}}^2(\alpha)$.

kinetic model, the impurity never shows steady-state diffusion with respect to the granular gas where it is immersed (even in a strongly sheared system).

In order to characterize the nonequilibrium state of the impurity, we have selected a number of relevant dimensionless coefficients. The basic one is the temperature ratio $\chi = T_1/T_2$, quantifying the lack of energy equipartition between both species. The momentum flux defines three independent coefficients: the nonlinear shear viscosity η_1, equation (3.47), and the two viscometric coefficients (or normal stress differences) N_1 and M_1, equation (3.48). Similarly, the heat flux defines the nonlinear thermal conductivity λ_1 and the cross-coefficient ϕ_1, equation (3.49). Notice that the coefficients N_1, M_1 and ϕ_1 do not have counterparts at the NS level. In particular, the coefficient ϕ_1 is interesting because it accounts for a component of the heat flux orthogonal to the thermal gradient, induced by the shearing.

Comparison between the exact solution and the DSMC simulations shows a good agreement, thus indicating the existence of a hydrodynamic or normal solution, even under extreme conditions, beyond the NS regime. The results show that, in general, T_1 is higher (lower) than T_2 if m_1 is larger (smaller) than m_2. Moreover, as expected, the deviation of the temperature ratio χ from unity increases as the inelasticity and/or the
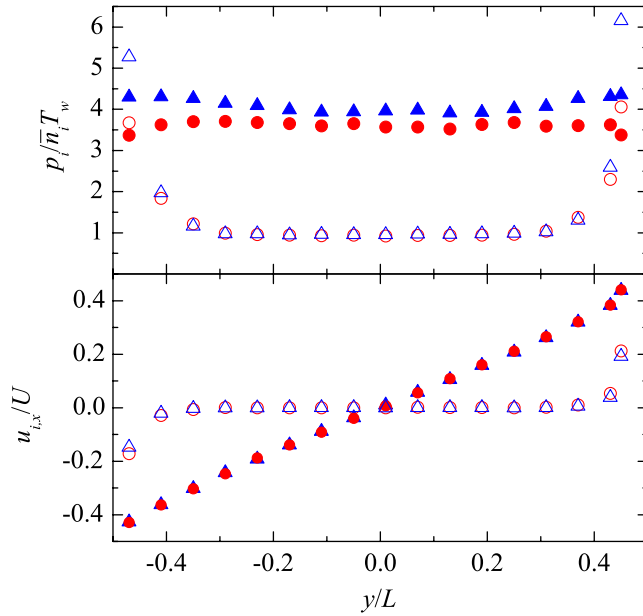
Figure 11. Pressure and flow velocity profiles for the impurity (triangles) and the gas particles (circles) at $t \approx \overline{\tau}$ (open symbols) and $t \approx 10^3 \overline{\tau}$ (filled symbols). The system corresponds to $\alpha_{12} = \alpha_{22} = 0.9$, $m_1/m_2 = 2$, $\sigma_1/\sigma_2 = 1$, $L = 7.14\overline{\ell}$ and $U = 10v_0$. The data have been obtained from DSMC simulations of the Boltzmann equation.

shear rate increase. Concerning the generalized coefficients η_1 and λ_1, it is observed that both decrease as the shear rate increases, while they increase with increasing dissipation and mass ratio m_1/m_2. As expected, the anisotropy of the normal stresses increases as the shear rate increases. In addition, as the impurity becomes heavier, the difference between the xx and yy stresses increase, while the difference between the zz and yy stresses decrease. The latter effect is also present when the system becomes more inelastic. Finally, in general, the cross-coefficient ϕ_1 does not present a monotonic dependence on the shear rate. However, like in the cases of η_1 and λ_1, the coefficient ϕ_1 increases as the mass of the impurity and/or dissipation increases. Interestingly, the latter effect is so remarkable that ϕ_1 can be larger than λ_1 (and hence $|q_x| > |q_y|$) if the impurity is sufficiently massive or the system is sufficiently inelastic.

The work carried out in this paper can be extended along several lines. On the one hand, since the states considered here have been restricted to conditions where $\gamma > 0$ ($a > a_{\rm th}$), it would be desirable to extend the analysis to the complementary situations where $\gamma < 0$ ($a < a_{\rm th}$, shaded region in figure 2). While the simulation method does not present any technical difficulty in the latter case, the analytical solution found in this paper involves $\sqrt{\gamma}$ (see, for instance, equations (3.12)–(3.15)) and so is not mathematically well defined when $\gamma < 0$. However, we have observed that an analytical continuation of the solution accounts well for the simulation results for a range of negative values of γ [52]. Another possible alternative to overcome this technical difficulty is to carry out a perturbation solution in powers of γ, exploiting the fact that $|\gamma|$ is a small parameter in the region $a < a_{\rm th}$, as preliminary computer simulation results show. A second interesting

problem is the extension of the tracer limit results derived here to a general bidisperse mixture with arbitrary composition. The main idea would be to guess hydrodynamic profiles for the mixture similar to those of a monodisperse system [37], along with a common flow velocity and uniform mole fractions and temperature ratios. Finally, the theoretical results predicted by the kinetic model will be confronted with those obtained by DSMC simulations of the true Boltzmann equation. Our preliminary results show that the good agreement found in the monodisperse case [37] extends to the case of mixtures, at least at a semi-quantitative level.

Acknowledgments

Appendix. Transport properties associated with the impurity at the threshold shear rate

In this appendix we derive the explicit expressions for the transport coefficients of the impurity along the threshold shear rate $a_{\text{th}}(\alpha_{22})$. They are obtained by taking the limit $\gamma \to 0^+$ in the corresponding expressions of section 3. A similar study was carried out in [53] by applying Grad's method to the Boltzmann equation.

First, note that when $y \to 0^+$ the function $\theta(w, y, z)$ defined by equation (3.15) goes to infinity, so that one can make use of the asymptotic expansion of the complementary error function [54], i.e.

$$\sqrt{\pi}\theta e^{\theta^2}\text{erfc}(\theta) \approx 1 - \frac{1}{2\theta^2}, \qquad \theta \gg 1. \tag{A.1}$$

Inserting this expansion into equation (3.13) and performing the integral, one obtains

$$F_{0,m}(y,z) \approx -\frac{4m!}{z^2}\left[(1+z)^{-(1+m)} + (1+2z)^{-(1+m)} - 2^{2+m}(2+3z)^{-(1+m)}\right]y, \qquad y \ll 1. \tag{A.2}$$

Since $F_{1,m}(y,z) = y\partial F_{0,m}(y,z)/\partial y$, it follows that $F_{1,m}(y,z) \approx F_{0,m}(y,z)$ to first order in y. Furthermore, the functions $X(\theta)$ and $Y(\theta)$ defined by equations (3.25) and (3.26), respectively, behave as

$$X(\theta) \approx \frac{1}{\theta}, \qquad Y(\theta) \approx \frac{3}{2\theta}, \qquad \theta \gg 1. \tag{A.3}$$

Therefore,

$$G(y,z) \approx \frac{d+4}{z}\left[-(1+2z)^{-2} + 4(2+3z)^{-2}\right]\sqrt{2y}, \qquad y \ll 1, \tag{A.4}$$

$$H(y,z) \approx \frac{18}{z}\left[-(1+2z)^{-4} + 16(2+3z)^{-4}\right]\sqrt{2y}, \qquad y \ll 1. \tag{A.5}$$

Since both $F_{0,m}(\widetilde{\gamma}, \widetilde{\zeta}_1)$ and $F_{1,m}(\widetilde{\gamma}, \widetilde{\zeta}_1)$ go to zero when $\gamma \to 0$, equation (3.44) becomes

$$d \left(\frac{T_1}{T_{12}} - \frac{1}{1 + \widetilde{\zeta}_1} \right) - \frac{2\widetilde{a}_{\mathrm{th}}^2}{(1 + \widetilde{\zeta}_1)^3} = 0. \tag{A.6}$$

This is a fourth-degree algebraic equation whose physical solution gives the temperature ratio χ in the simple shear flow. Once χ is known, the transport coefficients are readily obtained. The coefficients associated with the momentum transport are, from equations (3.50)–(3.52),

$$\eta_1 = \frac{T_{12}}{T_1} \frac{\chi}{(1 + \widetilde{\zeta}_1)^2}, \tag{A.7}$$

$$N_1 = 2 \frac{T_{12}}{T_1} \frac{\widetilde{a}_{\mathrm{th}}^2}{(1 + \widetilde{\zeta}_1)^3}, \qquad M_1 = 0. \tag{A.8}$$

The evaluation of the generalized thermal conductivity λ_1 at $\gamma = 0$ from equation (3.53) is trickier than before since substitution of equation (A.7) into (3.53) yields an indeterminate result. This difficulty is circumvented by first eliminating $\widetilde{a}^2$ between equations (3.44) and (3.53) and replacing η_1 by its expression (3.50). The result expresses λ_1 in terms of the functions $F_{0,m}(\widetilde{\gamma}, \widetilde{\zeta}_1)$ and $F_{1,m}(\widetilde{\gamma}, \widetilde{\zeta}_1)$. Then, the asymptotic value (A.2) is used and the limit $\widetilde{\gamma} \to 0$ is taken. The final result is

$$\lambda_1 = \left(\frac{T_{12}}{T_1} \right)^2 \frac{2\chi^2}{2 + 7\widetilde{\zeta}_1 + 6\widetilde{\zeta}_1^2} \left[1 + \frac{6}{d+2} \frac{12 + 42\widetilde{\zeta}_1 + 37\widetilde{\zeta}_1^2}{(2 + 7\widetilde{\zeta}_1 + 6\widetilde{\zeta}_1^2)^2} \widetilde{a}_{\mathrm{th}}^2 \right]. \tag{A.9}$$

The limit $\gamma \to 0$ of the cross-coefficient ϕ_1 is easily obtained from equation (3.54) as

$$\phi_1 = \frac{2}{d+2} \left(\frac{T_{12}}{T_1} \right)^2 \chi^2 \frac{4 + 7\widetilde{\zeta}_1}{(2 + 7\widetilde{\zeta}_1 + 6\widetilde{\zeta}_1^2)^2} \widetilde{a}_{\mathrm{th}} \left[d + 4 + 18 \frac{8 + 28\widetilde{\zeta}_1 + 25\widetilde{\zeta}_1^2}{(2 + 7\widetilde{\zeta}_1 + 6\widetilde{\zeta}_1^2)^2} \widetilde{a}_{\mathrm{th}}^2 \right], \tag{A.10}$$

where use has been made of equations (A.4) and (A.5). Despite the fact that there is no heat flux in the simple shear flow, equations (A.9) and (A.10) are intrinsic transport coefficients characterizing the state of the system. Equations (A.7)–(A.10) also describe the transport properties of the Couette flow with a temperature profile linear in s.

Equations (A.7)–(A.10), when particularized to an impurity mechanically equivalent to the particles of the host gas, are consistent[2] with the results reported in appendix D of [37].

References

[1] Goldhirsch I, 2003 *Annu. Rev. Fluid Mech.* **35** 267
[2] Brilliantov N V and Pöschel T, 2004 *Kinetic Theory of Granular Gases* (Oxford: Oxford University Press)
[3] Jenkins J T and Mancini F, 1987 *J. Appl. Mech.* **54** 27
[4] Jenkins J T and Mancini M, 1989 *Phys. Fluids* A **1** 2050
[5] Zamankhan P, 1995 *Phys. Rev.* E **52** 4877
[6] Arnarson B and Willits J T, 1998 *Phys. Fluids* **10** 1324
[7] Willits J T and Arnarson B, 1999 *Phys. Fluids* **11** 3116

---

[2] Note, however, that equation (D4) of [37] is restricted to a three-dimensional gas.

[8] Serero D, Goldhirsch I, Noskowicz S H and Tan M-L, 2006 *J. Fluid Mech.* **554** 237
[9] Martin P A and Piasecki J, 1999 *Europhys. Lett.* **46** 613
[10] Garzó V and Dufty J W, 1999 *Phys. Rev.* E **60** 5706
[11] Barrat A and Trizac E, 2002 *Granul. Matter.* **4** 57
[12] Garzó V, 2006 *Europhys. Lett.* **75** 521
[13] Montanero J M and Garzó V, 2002 *Granul. Matter.* **4** 17
[14] Dahl S R, Hrenya C M, Garzó V and Dufty J W, 2002 *Phys. Rev.* E **66** 041301
[15] Pagnani R, Bettolo Marconi U M and Puglisi A, 2002 *Phys. Rev.* E **66** 051304
[16] Paolotti D, Cattuto C, Bettolo Marconi U M and Puglisi A, 2003 *Granul. Matter.* **5** 75
[17] Krouskop P E and Talbot J, 2003 *Phys. Rev.* E **68** 021304
[18] Wang H Q, Jin G J and Ma Y Q, 2003 *Phys. Rev.* E **68** 031301
[19] Brey J J, Ruiz-Montero M J and Moreno F, 2005 *Phys. Rev. Lett.* **95** 098001
[20] Brey J J, Ruiz-Montero M J and Moreno F, 2006 *Phys. Rev.* E **73** 031301
[21] Schröter M, Ulrich S, Kreft J, Swift J B and Swinney H L, 2006 *Phys. Rev.* E **74** 011307
[22] Wildman R D and Parker D J, 2002 *Phys. Rev. Lett.* **88** 064301
[23] Feitosa K and Menon N, 2002 *Phys. Rev. Lett.* **88** 198301
[24] Garzó V and Dufty J W, 2002 *Phys. Fluids* **14** 1476
[25] Garzó V, Montanero J M and Dufty J W, 2006 *Phys. Fluids* **18** 083305
[26] Garzó V and Montanero J M, 2007 *J. Stat. Phys.* **129** 27
[27] Garzó V, Dufty J W and Hrenya C M, 2007 *Phys. Rev.* E **76** 031303
     Garzó V, Hrenya C M and Dufty J W, 2007 *Phys. Rev.* E **76** 031304
[28] Brey J J, Ruiz-Montero M J, Cubero D and García-Rojo R, 2000 *Phys. Fluids* **12** 876
[29] Garzó V and Montanero J M, 2004 *Phys. Rev.* E **69** 021301
[30] Montanero J M and Garzó V, 2003 *Phys. Rev.* E **67** 021308
[31] Garzó V and Montanero J M, 2003 *Phys. Rev.* E **68** 041302
[32] Santos A, Garzó V and Dufty J W, 2004 *Phys. Rev.* E **69** 061303
[33] Richman M W and Chou C S, 1988 *J. Appl. Math. Phys.* **39** 885
[34] Hanes T N, Jenkins J T and Richman M W, 1988 *J. Appl. Mech.* **55** 969
[35] Lun C K K, 1996 *Phys. Fluids* **8** 2868
[36] Babic M, 1997 *Phys. Fluids* **9** 2486
[37] Tij M, Tahiri E E, Montanero J M, Garzó V, Santos A and Dufty J W, 2001 *J. Stat. Phys.* **103** 1035
[38] Liu X, Metzger M and Glasser B J, 2007 *Phys. Fluids* **19** 073301
[39] Vega Reyes F, Garzó V and Santos A, 2007 *Phys. Rev.* E **75** 061306
[40] Brey J J, Dufty J W, Kim C S and Santos A, 1998 *Phys. Rev.* E **58** 4638
[41] Garzó V and Dufty J W, 1999 *Phys. Rev.* E **59** 5895
[42] Vega Reyes F and Urbach J S, 2008 *J. Fluid Mech.* submitted [arXiv:0807.5125]
[43] Brey J J, Dufty J W and Santos A, 1999 *J. Stat. Phys.* **97** 281
[44] Montanero J M, Santos A and Garzó V, 2000 *Phys. Fluids* **12** 3060
[45] Bird G I, 1994 *Molecular Gas Dynamics and the Direct Simulation of Gas Flows* (Oxford: Clarendon)
[46] Alexander F J and Garcia A L, 1997 *Comput. Phys.* **11** 588
[47] See the website http://cache-www.intel.com/cd/00/00/34/76/347649_347649.pdf
[48] Du Y, Li H and Kadanoff L P, 1995 *Phys. Rev. Lett.* **74** 1268
     Grossman E L, Zhou T and Ben-Naim E, 1997 *Phys. Rev.* E **55** 4200
     Kudrolli A, Wolpert M and Gollub J P, 1997 *Phys. Rev. Lett.* **78** 1383
     Brey J J and Cubero D, 1998 *Phys. Rev.* E **57** 2019
[49] Garzó V and Santos A, 1993 *Phys. Rev.* E **48** 256
[50] Garzó V and Santos A, 2003 *Kinetic Theory of Gases in Shear Flows. Nonlinear Transport*
     (Dordrecht: Kluwer–Academic)
[51] Vega Reyes F, Santos A and Garzó V, 2008 in preparation
[52] Vega Reyes F, Garzó V and Santos A, *Rheological properties of a granular impurity in the Couette flow*,
     2008 *15th Int. Congress on Rheology* (*AIP Conf. Proc.* vol 1027) ed A Co *et al* (Melville, NY: AIP)
     pp 953–5
[53] Garzó V, 2002 *Phys. Rev.* E **66** 021308
[54] Abramowitz M and Stegun I A (ed), 1972 *Handbook of Mathematical Functions* (New York: Dover)